1 Introduction

The recovery of the CMB anisotropy pattern and, in particular, of its statistical representation in terms of angular power spectrum (APS) generally requires to disentangle the CMB component from the foreground. This process is based from one side on the state-of-the-art knowledge of the Galactic and extragalactic components and from the other on the development of precise algorithms to separate the CMB from the foreground in the microwave maps, possibly complemented by anchillary information at other frequencies. The case of polarization data, with respect to that of total intensity - or temperature - data, exibits a relevant intrinsic complication related to the fact that while Galactic foreground components are typically polarized up to 5-50%, the CMB aniotropies are only weakly polarized (few %) and in particular, the CMB B-mode is much weaker than the E-mode, differently from the case of foregrounds where these two polarization modes have almost the same amplitude. On the contrary, a relevant simplification comes from the fact that the free-free emission is intrinsically not polarized.

In this chapter we present a comprehensive review of the current understanding of polarized foregrounds from the point of view of the information available by observations at various frequency bands (Sects. 2 and 3) and from the astrophysical point of view (Sect. 8). The level of foreground polarization anisotropy is compared with that of the CMB one, with emphasis the the B-mode. We discuss also the kind of information expected in the next years from forthcoming and future survyes that will allow to improve our current picture (Sect. 4). While the APS is certainly the most significant statistical estimator for the BPOL main science, we note also that in the context of a high sensitivity polarization mission like BPOL also the non Gaussianities of foreground and, possibly, of the CMB need to be taken in consideration (Sect. 5). In Sect. 6 we review the available methods to separate the CMB from the foreground diffuse components and their expected quality applied to BPOL while the implications of the point source subtraction is discussed in Sect. 7. Sect. 9 is devoted to the understanding of the foreground residual contamination in the CMB maps and then in the CMB APS to provide, in particular, an estimate of the ultimate astrophysical limitation to the detection and study of the B-mode. Finally, in Sect. 10 we summarize the main implication of this study for the BPOL design and discuss the expected BPOL main science expectation in the view of foreground limitation and in Sect. 11 we address the BPOL capabilities of improving our knowledge of the polarization properties of Galactic and extragalactic components.

2 Galactic foregrounds

2.1 Anchillary data

2.1.1 Polarized synchrotron emission: information from radio surveys

A number of large-scale ground based polarization surveys were carried out in the sixties and seventies in the frequency range up to 1.4 GHz (see Reich (2007) for a review). The only all-sky polarization survey is at 1.4 GHz and was recently completed (Fig. 1)., which is combined from a northern sky survey (Wolleben et al., 2006) and a southern sky map (Testori et al., 2007). The survey is at 0.6° angular resolution and it takes absolute temperatures from the early Dwingeloo survey (Brouw & Spoelstra, 1976) for offset calibration into account. Comparing the 1.4 GHz PI map with the 22.8 GHz WMAP all-sky PI map shows a good correspondance for local Galactic features, but clearly indicates significant depolarization at 1.4 GHz towards the inner Galaxy, which ranges in latitude up to about 30°. In fact rotation measures (RM) of the diffuse Galactic emission as revealed by the early low frequency Dwingeloo surveys show quite small RMs when compared with that of extragalactic sources, which show an increase to much higher values

along the Galactic plane. Surveys with arcmin angular resolution have been made at 1.4 GHz and 2.3/2.7 GHz, but are limited to a few degree wide stripe along the Galactic plane. These maps show a large number of structures not related to any total intensity structure, which again indicates the presence of Faraday rotation effects in the magneto-ionic medium along the line-of-sight. Although Faraday effects in these Galactic surveys will disappear at high enough frequencies, the Galactic plane is certainly not a good target for CMB observations.

However, at high enough latitudes Galactic Faraday effects are in general not important at 1.4 GHz, when analysing the total intensity and linear polarization survey in terms of the APS (La Porta 2007, La Porta et al. 2006). The B–mode peak at $l \sim 100$ may be detectable at 70 GHz. There are also a limited number of arcmin resolution polarization observation of high latitude patches available with promising results. Among high Galactic latitude regions, a relevant role to search the CMB B–mode can be played by the lowest emission regions. These can be located by using the WMAP data (Carretti et al. 2006b) and are found to extend some 20% fraction of the sky. However, the low S/N-ratio of the WMAP data allows estimates of the synchrotron emission only by angular extrapolations (see Sects. 2.2 and 2.3.1) and better analysis are needed. The frequency behaviour of the synchrotron emission makes it easier to detect and to characterize these regions at radio wavelenghts, provided that the frequency is high enough to prevent Faraday rotation modulations and that the observations are sensitive enough.

First deep observations have been carried out in small areas (< 10 deg^2) in the target fields of CMB experiments like BOOMERanG, BaR-SPOrt, and DASI (Carretti et al. 2005, Carretti et al. 2006, Bernardi et al. 2006) with promising results. The comparison with the 1.4 GHz northern sky survey (Wolleben et al., 2006) shows that these selected areas feature a signal 10+ times weaker than the general high Galactic latitude emission. This is significantly lower and would improve by a factor 100+ the detection limit of the T/S ratio. Implications for the cosmic B-mode detection will be discussed in Sects. 9 and 9.3. Here it is just worth noting that measurements in special areas look thus be an appealing option, especially in case of low T/S values, provided they are large enough to keep under control the cosmic variance contribution.

Analysis of more extended regions are needed to understand the actual contamination in all of that best 20% sky fraction. Analysis of the WMAP data and on-going and future radio survey can fill the gap of information. They will be discussed in later sections.

Using a set of compilations of measurements for extragalactic radio sources, Dineen & Coles (2005) have constructed all-sky maps of the Faraday Rotation produced by the Galactic magnetic field. As long as relatively small multipoles are used the resulting maps are quite stable to changes in selection criteria for the sources, and show clearly the structure of the local Galactic magnetic field. They also suggested the use of these maps as templates for CMB foreground analysis, illustrating the idea with a cross-correlation analysis between the Wilkinson Microwave Anisotropy Probe (WMAP) data and the RM maps.

2.1.2 Starlight Polarization Surveys

Observed starlight polarization is believed to be caused by selective absorption by magnetically aligned interstellar dust grains along the line of sight. Since these measurements are limited by dust extinction, they provide us with a picture of the magnetic field only in the vicinity of the sun. Despite this limitation, recent analyses of such measurements (see [Heiles (2000), Fosalba et al. (2002)] and references therein) suggest that they do contain information about the uniform and random components of the magnetic field on large scales. In particular,starlight polarization vectors trace [Zweibel & Heiles (1997)] the plane-of-the-sky projection of the Galactic magnetic field and measurements of polarization for stars of different distances reveals the 3D distribution of magnetic field orientations averaged along the line of sight.

The starlight polarization data used is taken from the compilation by Heiles (see [Heiles (2000)] for details and references to the original catalogues; see also [Fosalba et al. (2002)]). This com-

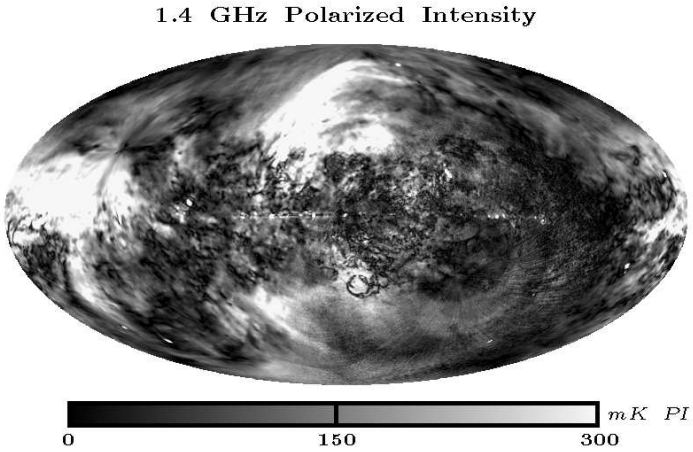

Figure 1: All-sky survey of linearly polarized intensities at 1.4 GHz displayed in Galactic coordinates. The surveys sensitivity is 15 mK and its angular resolution 36 arcmin. Strong depolarization is seen within about +/- 30 deg Galactic latitude towards the central region of the Galaxy.

pilation includes data from 9286 sources taken from a dozen of catalogs combining multiple observations, providing accurate positions and reliable estimates for extinction and distance of stars. From this catalog, we have selected a subsample of 5513 stars (60% of the data) which have small polarization degree errors and include extinction information.

Latitude	Distance	Stars (%)	P(%)	E(B-V)
Low Latitude	Total	4114(75)	1.69	0.49
	Nearby	1451(26)	0.94	0.29
	Distant	2663(48)	2.09	0.60
High Latitude	Total	1399(25)	0.45	0.15
	Nearby	1315(24)	0.42	0.14
	Distant	84(1)	0.89	0.26

Table 1. Mean Stellar Parameters. High latitude (low latitude) means $|b| > 10^\circ$ ($|b| < 10^\circ$) and nearby (distant) denotes $d < 1kpc$ ($d > 1kpc$). The quantities between brackets denote amount % of all stars in the sample.

practically all high latitude ($|b| > 10^\circ$) stars are nearby ($d < 1kpc$). Within the Galactic plane one can find relatively distant stars, though the vast majority are within 2 kpc. Therefore, this is a rather local sample. This is also clearly displayed in the starlight polarization map of the subsample of 5513 stars analyzed (see Fig 2).

A more quantitative account of this fact is summarized in Table 1, where we give the mean stellar parameters (i.e, polarization degree P(%) and extinction as measured by the color excess E(B-V)) in the subsample as a function of latitude and distance. It is seen that low-latitude stars have large values of the polarization degree P(%) ≈ 1.7, and extinction E(B-V) ≈ 0.5, while high-latitude sources exhibit significantly lower values, P(%) ≈ 0.5, E(B-V) ≈ 0.15. Polarization vectors (defined with respect to Galactic coordinates) are typically oriented along the Galactic plane ($\theta_p \approx 90^\circ$) although a more detailed analysis reveals a rich spatial distribution (see Fig. 2)

As shown in Fig. 2, there is a strong net alignment of starlight polarization vectors averaged over many clouds with the Galactic plane structures (see lower panel) as well as a clear alignment

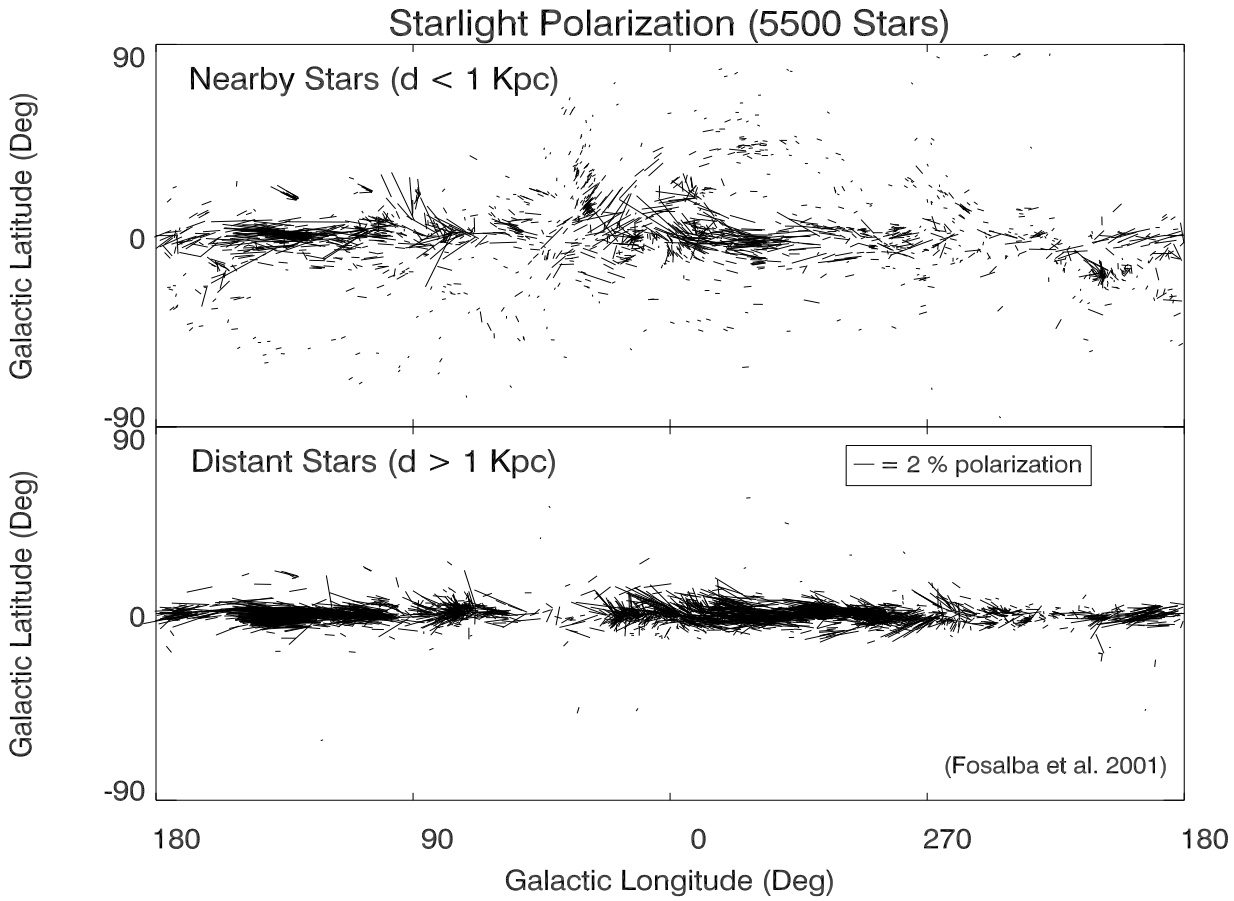

Figure 2: Starlight polarization vectors in Galactic coordinates for a sample of 5513 stars. The upper panel shows polarization vectors in local clouds, while the lower panel displays polarization averaged over many clouds in the Galactic plane. The length of the vectors is proportional to the polarization degree and the scale used is shown in the lower panel.

with the spherical shell of Loop 1 as seen from the polarization vectors in local clouds (see upper panel).

On the other hand, the spatial distribution of the polarization degree and position angle are expected to be highly correlated and this is also observed in the starlight polarization map (Fig 2), where highly polarized regions exhibit position angles aligned with the Galactic plane, following the plane-of-the-sky projection of the various Galactic spiral arms.

What does it tell us about the galactic magnetic field? It is generally accepted that grains in diffuse interstellar gas tend to be aligned with their major axes perpendicular to the magnetic field. According to the radiative torque mechanism, the electric field of radiation transmitted by an interstellar dust grain is less absorbed along the grain minor axis and therefore polarized in that direction (i.e, polarization results from *differential absorption*) which is parallel to the external magnetic field orientation. Thus, polarized starlight radiation vectors are oriented parallel to the Galactic magnetic field [Zweibel & Heiles (1997)]. However, since starlight polarization vectors are only seen as projected in the plane of the sky, they just give us direct information on the plane-of-the-sky projection of the Galactic magnetic field orientation.

Therefore, we find evidence that *there is a net alignment of the magnetic field (as seen from its plane-of-the-sky projection) with Galactic structures on large-scales.* However, the full reconstruction of the 3D magnetic field orientations (and strength) requires additional complementary data from radio (synchrotron), sub-mm/IR (dust) observations and rotational measures from distant pulsars.

2.1.3 FIR/submm surveys

2.1.3.1 The Archeops survey

Archeops (Benoît et al. [Benoit et al. (2002)]) was a balloon–borne instrument dedicated to measuring cosmic microwave background (CMB) temperature anisotropies at high angular resolution (about 10 arcminutes) over a large fraction (30%) of the sky in the (sub)millimetre domain (from 143 to 545 GHz). The Archeops data collected during the last flight of the experiment that occured during the Arctic night from Kiruna (Sweden) to Russia in February 2002 have allowed the first large scale detection of polarized dust emission in our Galaxy.

Polarized results of Archeops have been published in Benoît et al. [Benoit et al. (2004a)]. Archeops was equipped with six bolometers operating at at 353 GHz assembled in three Ortho Mode Transducers (OMT). Using the 3 pairs of bolometers allowed reconstruction of the linear polarization information (polarization degree p and polarization angle ψ), using the differences between signals from the various bolometers. The polarized sky emission detected by Archeops at 353 GHz is dominated by the linearly polarized thermal dust emission. It is due to non-spherical dust grains being aligned on large scales in the ISM, through their interaction with the magnetic field. The degree of polarization was known to be weak (of the order of a few %) from previous observations. It is worth noticing, however, that those measurements were generaly obtained towards much brighter regions than those observed by Archeops.

A significant polarized signal was detected in the Archeops data towards several individual regions of the sky. Those regions are located along the Galactic Plane, where the intensity is high enough that the polarization can be measured. They correspond to individual Molecular Clouds (MCs). The polarization degree towards those regions is larger than 5%, much stronger than previously expected, and is sometimes larger than has ever been measured toward any region of the sky before (consistant with p up to 10%). Note that these figures are average values taken over fairly large regions of the sky, of the order of 3-50 square degrees. Note also that currently available techniques from the ground do not presently allow the detection of polarization over such large areas with moderate to low intensity. The reason for such large polarization values in individual clouds is still unclear. In principle, they may correspond to regions where the geometry of the magnetic field orientation is very coherent and close to the

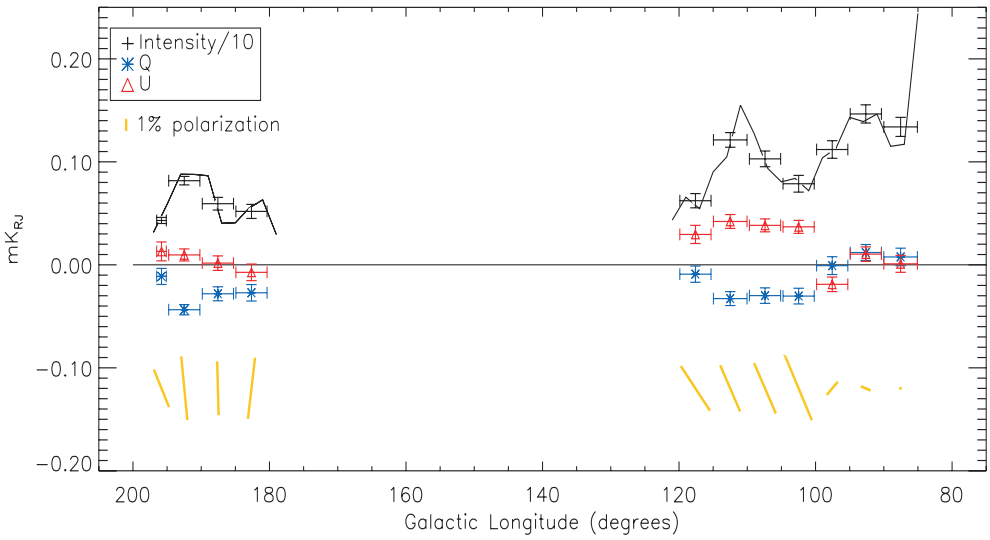

Figure 3: Diffuse galactic polarization: This figure shows the distribution of the Intensity as well as the Q and U stokes parameters with Galactic longitude. The lines in the lower half show the polarization direction and polarization fraction distribution. It can be seen that the polarization is mostly perpendicular to the Galactic plane and vanishes in the Cygnus region, near $l = 90$ deg.

plane of the sky over large volume areas. They could also correspond to molecular clouds where the dust properties vary and grain alignment is favored.

In addition to the above individual regions, the polarization of the extended GP emission was also detected, by averaging the signal into bands at various Galactic longitudes. Most regions show a diffuse polarization degree of the order of $4 - 5\%$, with the exception of the Cygnus region which show no measureable polarization, despite the fact that it is the brightest region of the map. The polarization direction is mainly orthogonal to the Galactic plane. This can be explained naturally if the magnetic field orientation is within the plane, as is the case for external elliptical galaxies similar to ours where the field is observed to follow the geometry of the spiral arms. This geometry is also supported by optical studies of the star light polarization in extinction (see Sect. 2.1.2). In this context, the absence of polarization towards the Cygnus region in the Archeops data can be explained, because this region corresponds to the tangent point where the GP is seen along the local spiral arm. In this direction, the magnetic field is pointing away from us, producing no apparent dust alignment and therefore no polarization.

2.1.3.2 The WMAP survey

2.1.3.3 The PILOT survey

PILOT (see http://pilot.cesr.fr) is a stratospheric balloon experiment designed to measure the polarization of thermal dust emission at $240\mu m$ (1.2 THz) an $550\mu m$ (545 GHz) with a resolution of a few arcminutes (see Bernard et al. [**?**]). The science case of PILOT is to map the B-field direction over a large fraction of the galactic plane ($|b| < 20$ deg) and towards faint diffuse cirrus clouds. The experiment will use bolometer arrays developped for the PACS experiment on board the Herschel sattelite. Although the sensitivity of such bolometers is still significantly less than that of TES bolometers, for instance, they are well adapted to balloon conditions where the performances are limited by the instrumental background. PILOT will use 1024 bolometers. Along with the fact that the $240\mu m$ channel is conveniently located near the peak of the thermal dust emission, and that the PILOT scanning strategy will allow to over-integrate on specific sky regions, the large number of detectors will allow to reach better

columns density sensitivity than Planck. PILOT should therefore be able to detect polarization of thermal dust towards the most diffuse interstellar clouds located at high galactic latitudes (called cirrus clouds), the regions of interest to CMB cosmology because they contain the least contamination by galactic foregrounds.

Although PILOT will not clean the sky for Bpol (it will cover a fraction of the high latitude sky and is not operated at CMB frequencies), PILOT will contribute a major step forward in understanding the galactic foregeround properties relevant to Bpol. In particular, PILOT will allow to obtain precious informations about the degree of alignment of large dust grains with respect to B in the local solar neighborhood. We will have an indication of how B is structured at high latitude, in particular in the large scale HI bubbles (including the local bubble we live in) which are the largest poluters of the high latitude sky. The Pilot survey will suffer less systematical bias than optical surveys which are limited by the number of available stars with significant extinction at high latitude.

Because PILOT samples a different wavelength range as the Planck polarized channels, combining the PILOT and Planck results at intermediate and high galactic latitudes will inform us as weither the polarization degree varies with wavelength. Two different classes of model are currently proposed to explain the FIR emission of thermal dust. The first class assumes emission by two types of grains (e.g. Finkbeiner et al. [**?**]) a cold component at $T \simeq 16\,K$ dominating the emission in the PILOT wavelength range and a very cold component at $T \simeq 9\,K$ dominating the emission at Planck frequencies. These two components would be composed of Graphite and Silicate respectively and should have somewhat different alignment properties. Variations of the polarization degree is therefore expected in such models (e.g. Vaillancourt [**?**]). The scond class of models explains the flatness of the observed galactic emission in the submm by the contribution of localized deffects in the amorphous material composing the dust grains (see Meny et al. [**?**]). In these models, the FIR to mm range is contributed by the same grains, and no variations of the polarization properties with wavelengths are expected, a situation obviously more favorable to CMB polarization cosmology. The combination of the PLanck and PILOT polarization data will allow to settle this important issue. Note that, this result will impact on the choice of the optimum band positions to adress foreground contamination with Bpol : a situation where polarization properties do not vary with wavelengths would favor selecting higher frequencies to measure the polarization of thermal dust emission, since dust emission would be stronger there, and high frequency channels would lead to a more compact instrument.

2.1.4 Extrapolations from anchillary data to microwaves

2.1.4.1 Analysis of selected sky areas

The extrapolation of results coming from ancillary data to the microwave regime is crucial in assessing the detectability of the CMB B-mode component. The knowledge of the foreground properties at frequencies different than the microwave regime allows to optimize experimental specifications like the best frequency window at which to observe, the number of frequency channels, the required angular resolution and the technique to separate the various components.

Ancillary data provide an important way of forecasting how important the microwave foreground emission is. It is well established that polarized microwave foregrounds consist of synchrotron and dust emissions, as Galactic components, and extragalactic polarized radio sources. An anomalous dust component is also probably present but its relevance is still a matter of debate.

In this section we will mainly focus on the knowledge of the diffuse synchrotron and dust components as they result from observations at frequencies respectively lower and higher than the microwave regime.

The synchrotron diffuse radiation coming from our Galaxy has not been sufficiently studied

in the past. The only available data set which covers a relevant fraction of sky have been the old Dwingeloo survey [64] for many years. Only in recent times data at higher frequency, with better sampling, better sky coverage and finer resolution have become available. The most relevant data for our purposes are:

- a survey of the Southern Galactic Plane [65] made with the Parkes telescope at 2.3 GHz with 10.4 arcmin resolution;
- a survey of the Northern Hemisphere at 1.4 GHz [66] with the DRAO telescope, with 36 arcmin resolution;
- observations of a $3^\circ \times 3^\circ$ sky region centered at RA $\alpha = 5^h$ and DEC $\delta = -49^\circ$ (inside the field observed by the BOOMERanG experiment) at 1.4 GHz with the Australia Telescope Compact Array (ATCA), with 3.5 arcmin resolution [67] and at 2.7 GHz with the Parkes telescope [68], with 5 arcmin resolution;
- observations of the two fields imaged by the DASI experiment at RA $\alpha = 23^h30^m$ and DEC $\delta = -55^\circ$ and at RA $\alpha = 00^h30^m$ and DEC $\delta = -55^\circ$ respectively, at 1.4 GHz [69] with ATCA, with 3.5 arcmin resolution;
- observations of a $3.2^\circ \times 3.2^\circ$ selected sky region centered at RA $\alpha = 10^h58^m$ and DEC $\delta = +42^\circ18'$ at 1.4 GHz with the Effelsberg telescope, with 9 arcmin resolution [70].

The first extrapolations of low frequency data has been made by [71] using Parkes data. They found that both the synchrotron E and B-modes follow power laws, $C_\ell \propto \ell^{-\alpha}$, with similar amplitudes and slopes. Their work was mainly focused on the CMB E-mode detection, then they extrapolated the synchrotron angular power spectrum to 60 GHz showing that the CMB E mode would be detectable for an optical depth to reionization $\tau = 0.2$. Unfortunately this result does not tell much about the possible CMB B-mode detection.

In fact, extrapolations from low frequencies are affected by limitations mainly due to the sky coverage and the frequency of the data themselves. For instance, Parkes data cover mostly the Galactic Plane which is normally cut out in the CMB analysis. Therefore, results coming from this area are likely to be a pessimistic forecast for the amount of foreground in the microwave regime.

In addition to this, all results from low frequency data are affected by uncertainties in the frequency spectral index as well as by the unknown amount of Faraday rotation and by depolarization effects. The usual extrapolation is performed by assuming a constant spectral index to scale the angular power spectra up to the microwave regime, therefore the spectral index will influence only the normalization of the angular power spectrum. This can look unrealistic since the spectral index depends upon the position in the sky. Anyway, simulated maps ([72]) showed that when variations of the spectral index are taken into account, the resulting power spectra do not show relevant variations - both in amplitude and in slope -, at least when the Galactic Plane is cut out. Therefore, the assumption of a position-independent spectral index for the synchrotron emission looks fair.

The evaluation of the amount of Faraday rotation and depolarization effects are more concerning issues. Depolarizations effects depend upon the considered angular scale. Data at low frequency have normally a better angular resolution with respect to the CMB experiments, then beam depolarization is usually not a problem. Faraday depolarization effects depend upon the frequency and are relevant when the medium is Faraday thick. The microwave regime is instead Faraday thin. Therefore, they can play a relevant role at frequencies around 1 GHz, but are completely irrelevant in the microwaves.

Pure Faraday rotation effects do not cause any depolarization, but, as showed by [73], they can considerably change the slope of the angular power spectrum, by transferring power on the characteristic scales where fluctuations in the interstellar medium are present.

All these factors make the extrapolation of low frequency data in the microwave regime rather difficult. A way of getting rid of pure Faraday rotation effects is to survey a fraction of sky as large as possible and to push the observations themselves at the highest possible frequency. Observations at higher frequencies also help to avoid Faraday depolarization effects.

The observations performed with the Parkes telescope, the ATCA and the Effelsberg telescope were planned to avoid those problems as much as possible by selecting sky regions at high Galactic latitudes, at the highest frequencies available, with good angular resolution, proper sampling and low total intensity emission. Also DRAO data show sky patches that suit these requirements. Therefore, the analysis of those data allows a safer and more robust forecast for the synchrotron foreground contamination in the microwave regime.

The DRAO data have been analysed by [74]. The authors selected three specific patches with low emission and expressed the synchrotron polarized angular power spectra in terms of power laws. The results are slightly dependent upon the patch considered, but they look similar in all the three patches. For the synchrotron B-mode power spectrum, [74] found an average amplitude of ~ 0.07 mK^2 at $\ell = 100$ and an average slope $\alpha = 2.85$. The synchrotron power spectra are extrapolated according to two different frequency spectral indexes $\beta = 2.8$ and $\beta = 3.0$. They found that the CMB B-mode is accessible for tensor to scalar power ratios $r \geq 0.5$ even without any foreground removal, but, assuming that the synchrotron foreground can be subtracted with a 5% accuracy, they state that the peak of the CMB B-mode is achievable for $r \sim 0.005$.

This result is similar to the results that emerge from the analysis of all the dedicated observations carried out in selected low total intensity regions. In all the regions observed with the Parkes telescope, the ATCA and the Effelsberg telescope found very low levels of synchrotron polarized emission. The analysis of those data showed that the synchrotron emission always follows reasonably power law behaviours. Results show amplitudes for the synchrotron B-mode power spectrum ranging from 201 μK^2 at $\ell = 500$ at 1.4 GHz in the Effelsberg data to 40 μK^2 at $\ell = 500$ at 2.3 GHz in the BOOMERanG region. Slopes are also similar, being $\alpha = 1.87$ for the BOOMERanG field and $\alpha = 1.74$ in the field observed with the Effelsberg telescope.

Data for the two DASI fields are not conclusive since only an upper limit for the polarized emission has been found. This upper limit corresponds to 80 μK^2 at $\ell = 2000$ and 36 μK^2 at $\ell = 2000$ for the two fields respectively.

A prediction about the synchrotron contamination on the CMB B-mode in the microvawe regime can be made for each of these fields by extrapolating the angular power spectra with a typical frequency spectral index. Authors that analysed those data chose a frequency spectral index $\beta = -3.1$.

Unfortunately these data do not cover the most interesting region for the CMB B-mode detection, that is the region around $\ell = 100$ where the CMB B-mode shows the peak which can be directly related to the energy scale of the Inflation. The angular power spectra computed on the data have therefore been extrapolated in the multipole space in order to cover also the region around $\ell = 100$. This extrapolation introduces a further uncertainty but is justified by the similarities that the synchrotron power spectra slopes show in all the different sky regions analysed.

Even taking into account uncertainties related extrapolations in frequency and angular space, the results from the extrapolations converge to an encouraging scenario for the CMB B-mode detection. CMB B-mode power spectra with $r \sim 0.01$ or even $r \sim 0.001$ show the same emission level of the synchrotron B-mode angular power spectra extrapolated at 90 GHz. These results do not consider any foreground removing strategy; when a proper synchrotron subtraction is performed, the residual power spectrum amplitude can be lowered by an additional factor 10 and those results appear even more robust.

Fig. 4 summarized the knowledge about the polarized synchrotron emission and shows the importance of ancillary data in accessing the detectability of the CMB B-mode component. According to thi result, values of $r \sim 0.01 - 0.05$ for the CMB B-mode seem to be accessible,

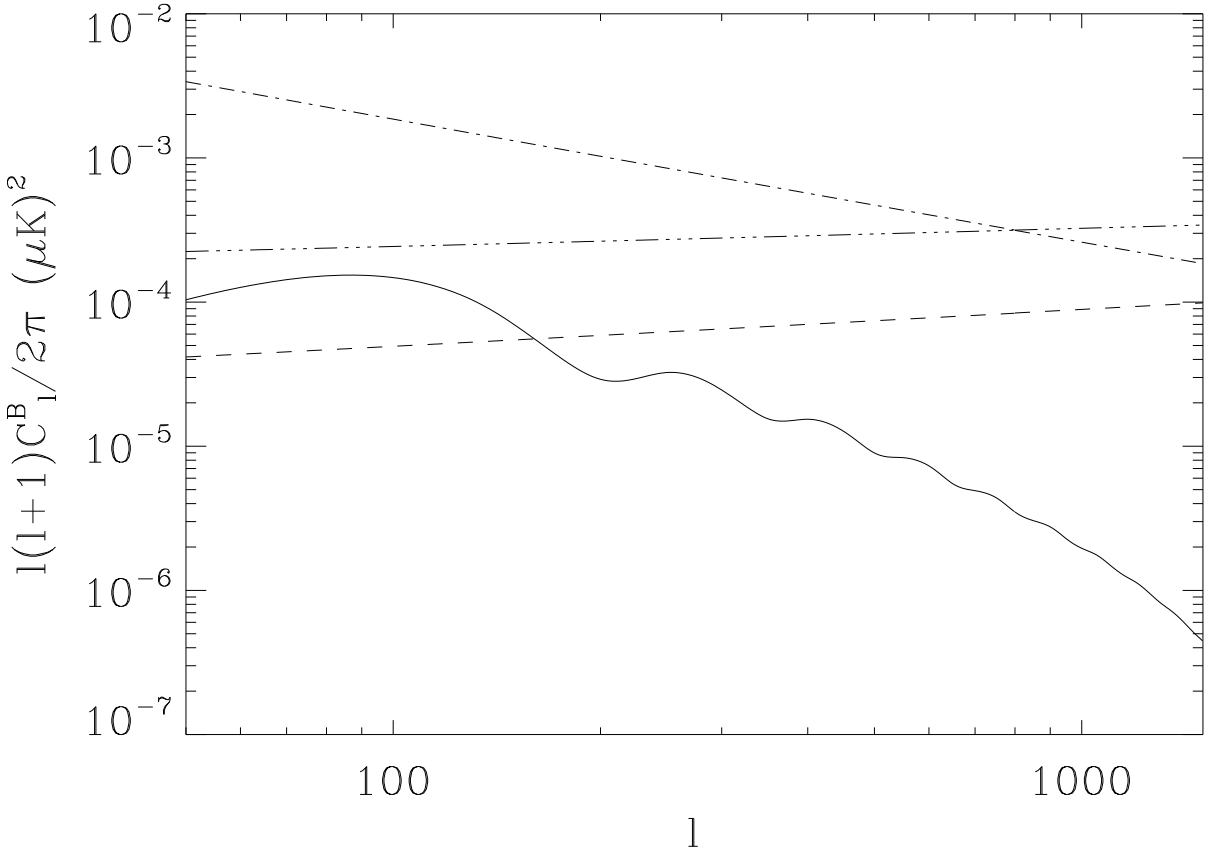

Figure 4: A comparison between the CMB B-mode power spectrum and synchrotron power spectra extrapolated from low frequency data at 70 GHz. The CMB B-mode (solid line) has a tensor to scalar power ratio $r = 0.01$ and the other cosmological parameters according to the concordance model. The synchrotron power spectra are showed for: Effelsberg data (dashed line), Parkes data (dashed triple-dotted) and DRAO data (dashed dotted). All the synchrotron spectra have been scaled in frequency assuming $\beta = -3.1$

at least in selected regions of the sky. This indication calls for larger and deeper observations in order to identify better the potential regions of investigations. Future observations will still be useful in combination with microwave data to constrain better the amount of foreground contamination.

So far we did not considered the contribution due to Galactic dust. In fact, the synchrotron emission is unlikely to be the dominant foreground component at 90 GHz where the dust should play a relevant role as well. Unfortunately, the observational information about polarized dust are even poorer than for the synchrotron emission. No survey of polarized Galactic dust exists so far and partial information can be extracted from the observations made by the Archeops experiment [75] even if their data cover a very limited region of sky and mainly in the Galactic Plane.

An evaluation of the dust contribution was attempted by [70]. They used total insentity data from the second BOOMERanG flight and chose two different dust polarization percentage of 5% and 10% according to the Archeops evidences at high Galactic latitudes. They also assumed a power spectrum power law for the dust $C_\ell \propto \ell^{-2}$ according to the WMAP results. The result is shown in Fig. 5 together with the contribution by the synchrotron emission.

From Fig. 5 can be seen that ancillary data helps in setting the optimal window frequency where looking for the CMB B-mode. This has a crucial impact in the experimental design

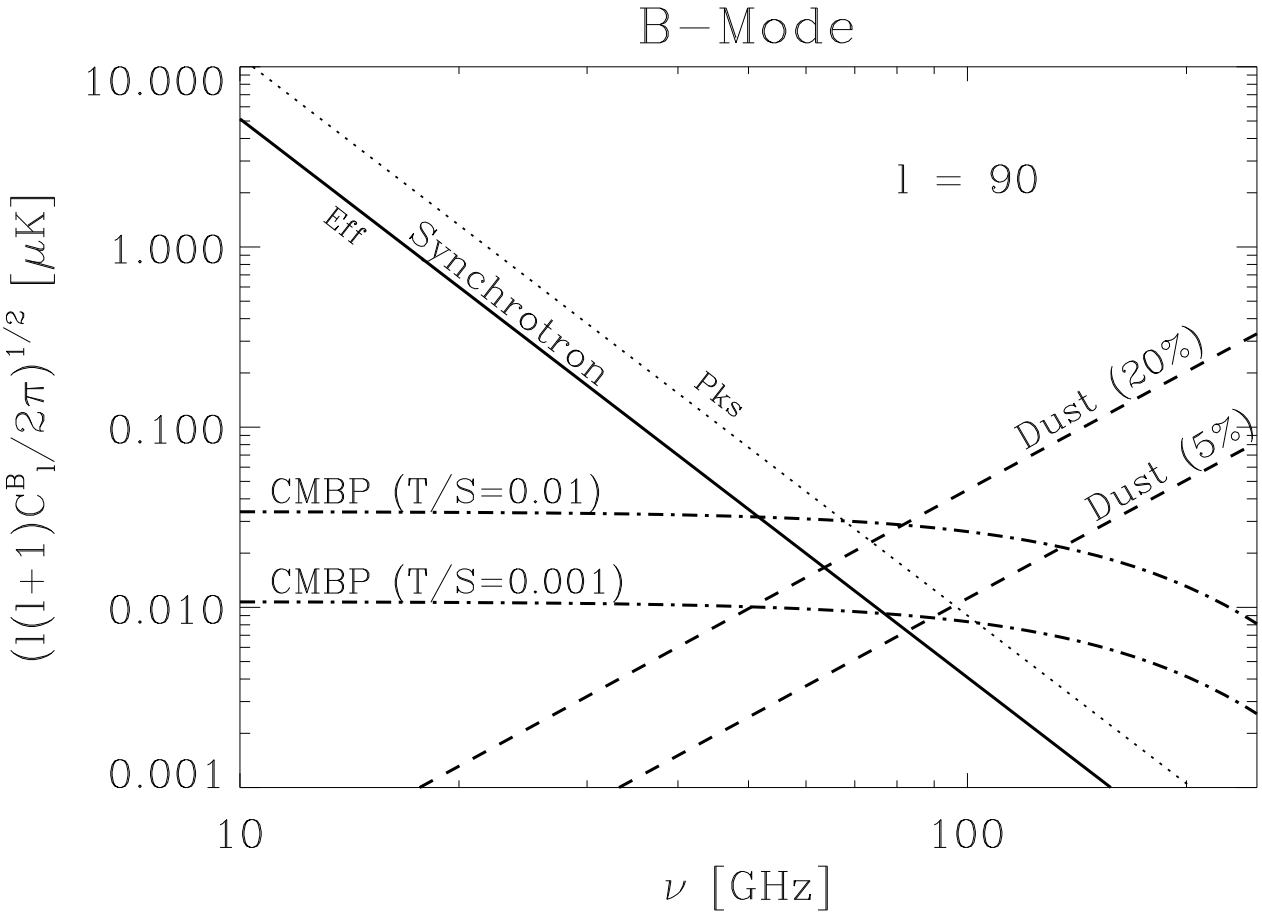

Figure 5: The frequency behaviour of the CMB polarization and the Galactic foregrounds estimated at $\ell = 90$. Two values of tensor to scalar power ratios are reported for the CMB B-mode. Two values of the synchrotron frequency spectrum are showed according to the normalization on the Effelsberg and Parkes data respectively. Estimates of polarized dust are also shown (the figure is taken from [70]).

and settings. In fact, these results seem to indicate that frequencies around 60-70 GHz are significantly free of synchrotron contamination and this might be a very good window frequency to look for the CMB B-mode. This result is not conclusive because it still misses reliable information from polarized dust but, however, suggests that the frequency window around 90-100 GHz is not the only one that shows a minimum in the foreground contamination. If the polarization percentage of the dust component will find to be at 10% or greater, than frequencies 60-70 GHz could even be the optimal choice for a clean detection of the CMB B-mode.

2.2 Galactic foregrounds from microwave surveys

2.2.1 Anomalous components

2.3 Nearly all-sky and local analyses

2.3.1 Information from WMAP

A direct way to estimate the foreground contamination to CMB B-mode measurements is to exploit the WMAP results. For the Q-, V- and W-band, the WMAP team released both the temperature and polarization maps derived from observations and a foreground cleaned version of those maps (Hinshaw et al. 2006; Page et al. 2006). The differences between the two

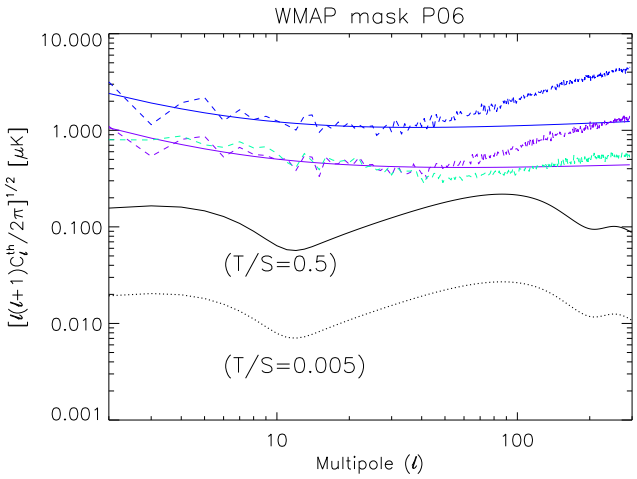

Figure 6: Comparison between the B-mode angular power spectra of the overall foreground emission in the Q-, V- and W-band (dark blue, violet and light blue lines, respectively) and the theoretical CMB B-mode for a concordance model with two values of the tensor-to-scalar ratio. The couloured solid lines are obtained by fitting the lower multipole range (ℓ $[3-30]$) of the foreground APSs with a power law and extrapolating the results to larger $\ll$'s.

versions of corresponding maps provide us with rough maps of the overall foreground emission, which in polarization is mostly due to the Galactic diffuse emission (synchrotron, dust) and to extragalactic sources. Fig. 6 shows the B-mode angular power spectrum (APS) derived from these foreground maps by applying a mask that excludes about 26% of the sky (essentially the Galactic plane regions and the North Polar Spur). A guess of the Galactic diffuse emission contaminating the WMAP measurements in the Q, V and W band can be obtained by fitting the lower multipoles range (ℓ $[3-30]$) with a simple power law and by extrapolating the results up to $\ell = 100$. The CMB B-mode for a concordance model in agreement with the WMAP 3-yr results is displayed for comparison.

The foreground signal turns out ot be larger by a factor ~ 2 than the CMB B-mode even for $T/S = 0.5$. Nevertheless, the analysis of Carretti et al. (2006) of the WMAP 3-yr K-band data suggests that the situation could be more favourable in particular areas, although at the cost of much less coverage. Fig. 7 shows the B-mode APS obtained for two patches, which cover respectively $\sim 20\%$ and ~ 10 of the sky in the northern hemisphere. Actually, the smaller is included in the larger one. In these cases, the v-band foreground emission is either comparable or about half the cosmological signal. Nevertheless, a component separation is most likely required to retrieve the CMB B-mode from observations.

3 Extragalactic foregrounds

The main emission mechanisms operating in extragalactic sources are synchrotron and thermal dust emission. Since the synchrotron emission spectrum generally decreases with increasing frequency, while that of dust emission steeply increases, the global spectral energy distribution of extragalactic sources has a deep minimum at wavelengths of a few millimeters, fortuitously close to the peak of the CMB spectrum. Although the two processes generally co-exist, their relative importance varies strongly between the different source populations. At $\nu \lesssim 100\,\mathrm{GHz}$ fluctuations are dominated by unresolved radio sources, which are substantially polarized and may therefore be a major contaminant of CMB polarization maps [34, 8, 35], primarily at large multipoles ℓ: if they are randomly distributed their rms contribution scales as ℓ. The available data indicate that clustering of radio sources is highly diluted because of their broad luminosity functions and redshift distributions and adds little to their fluctuation power spectra. On the

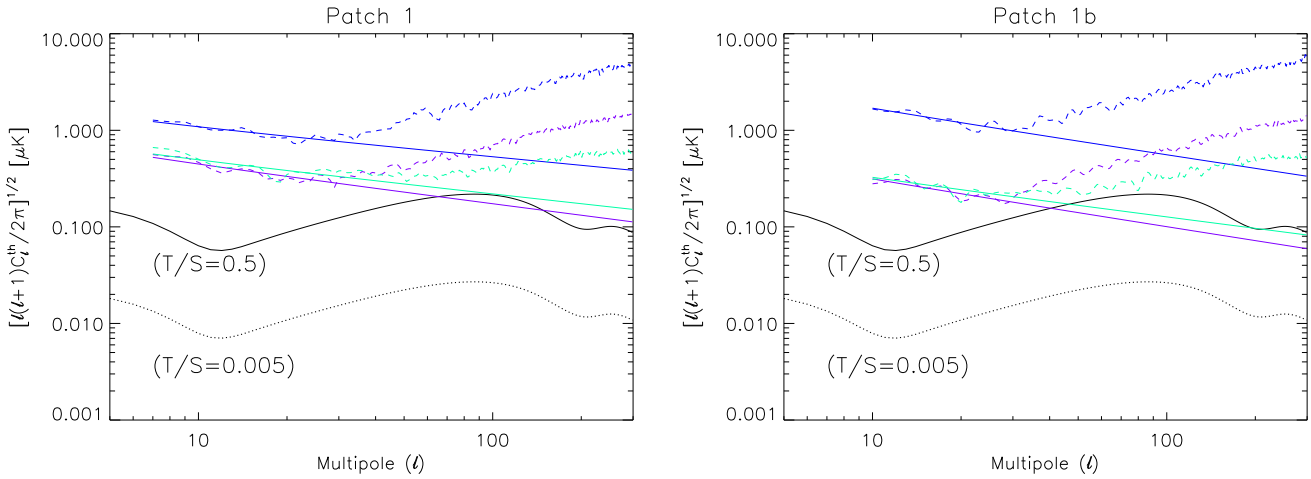

Figure 7: Comparison between the B-mode angular power spectra of the foreground emission in the Q-, V- and W-band (dark blue, violet and light blue lines, respectively) and the theoretical CMB B-mode for a concordance model with two values of the tensor-to-scalar ratio, for the two considered sky areas. The solid lines are the power law best fit over the lower multipole range and give an estimate of the contribution due to the Galactic diffuse emission.

other hand, the clustering of sub-millimeter bright galaxies, the sites of intense star formation activity, that dominate at higher frequencies, may be so strong [5, 30] to give the leading contribution to intensity fluctuations on scales from several arcminutes to $\simeq 1^\circ$ [24, 25]. Very little is known about their polarization, although some indications suggest that it may be weak. In the following sub-sections we will briefly review our current understanding of polarization properties of extragalactic sources.

3.1 Radio sources

The WMAP satellite [39] has recently provided the first all-sky surveys in the 20–100 GHz range. The information content of WMAP maps on polarization properties of extragalactic sources has not been exploited yet, and will anyway be limited to a small number of very bright radio sources.

Very useful additional is being provided by the Australia Telescope Compact Array (ATCA) 20 GHz survey of the Southern sky. Preliminary results on polarization of 173 sources in the declination range $-70^\circ < \delta < -60^\circ$, down to a flux limit of 100 mJy have been presented by [28, 29]. Most sources turned out to have low levels of linear polarization, with a median fractional polarization of 2.3%. A detailed investigation of polarization properties of a complete sample of the 183 brightest ($S_{20\mathrm{GHz}} > 500\,\mathrm{mJy}$) sources in the declination range $-30^\circ > \delta > -75^\circ$ is in progress ([6]).

A summary of pointed high radio frequency observations of low-frequency selected sources is presented in Table 1. An mean polarization degree of $\sim 2.5\%$, almost constant over the frequency range of 1.4–90 GHz, was found by [16] for a sample of 20 flat-spectrum sources. A similar median value ($\sim 2.3\%$) was reported by [26] for a complete sample of 93 flat-spectrum sources observed at 10GHz, while [3] found a median value of 5% at 14.5 GHz and 3.6% at 4.8 GHz for an incomplete sample of BL Lac objects.

A multifrequency (1.4, 2.7, 4.8, and 10.5 GHz) study of the B3-VLA sample (1050 sources selected at 408 MHz), including polarization measurements, was carried out by [14, 36]. The polarization properties of the sub-sample detected in polarization at 10.5 GHz were discussed by [18] who confirmed the earlier estimates of a median polarization degree of flat-spectrum sources $\simeq 2.5\%$, essentially constant from 2.7 to 10.5 GHz, but claimed that steep-spectrum sources have substantially higher polarization at 10.5 GHz ($\simeq 5.8\%$). The latter conclusion,

Project	Freq.(GHz)	Source No.	Selection criteria	Median fract. pol.
NVSS [7]	1.4	$\sim 2 \times 10^6$		$\sim 2\%$
Jones & al.(1985) [16]	1.4 - 90	20	flat-spectrum	2.5%
Okudaira & al.(1993) [26]	10.	93	flat-spectrum	2.3%
Aller & al.(1999) [3]	14.5	41	BL Lac objects	5%
	4.8	41	BL Lac objects	3.6%
B3-VLA [18]	1.4 - 10.5	1050		$1.9 - 4.6\%$ ($2.2 - 5.8\%$ for steep, $1.6 - 2.5\%$ for flat)
Ricci & al.(2004)[27]	18.5	258	Kühr sample	4.8% for steep, 2.7% for flat
Pilot-AT20G [28, 29]	20.	173	$-70 < \delta < 60$	2.3%
AT20G [6]	4.8-18	183	$\delta < 30$ $S_{20\mathrm{GHz}} > 500$ mJy	2.15% ($2.4 - 3.9\%$ for steep, $2.2 - 2.6\%$ for flat)

Table 1: Summary of the available observations of polarization in radio sources

however, is probably affected by selection effects.

Polarization measurements at 18.5 GHz of the 258 Southern sources in the Kühr sample [20], complete down to 1 Jy at 5 GHz, were carried out by [27]. The median fractional polarization for flat-spectrum sources was found to be $\sim 2.7\%$, while a higher polarization degree ($\sim 4.8\%$) was found for steep-spectrum sources, only a minority of which, however, had polarization measured. Again, the latter result may be affected by observational biases.

Much reacher data are available at low frequencies. The NVSS (NRAO VLA Sky Survey, [7]) data contain Stokes parameter information for 2×10^6 sources. The median fractional polarization, according to [34], is $\sim 2\%$, slightly dependent on the flux (with a hint of fainter steep-spectrum sources being more polarized) and on the spectral index.

3.2 Far-IR sources

Polarization data in the far-IR to sub-mm region are extremely poor. The brightest sources in polarization may be, again, the most powerful flat-spectrum radio sources, such as 3C279, for which polarized fluxes at $170\,\mu$m in the range 0.16–0.6 Jy have been measured with the ISO photo-polarimeter (ISOPHOT) by [17].

A map of polarized $850\,\mu$m dust emission in the starburst galaxy M82 has been obtained with SCUBA by [13]. Although individual regions are up to 9% polarized, the complex structure of the magnetic field results in very diverse polarization directions, yielding a much lower global average polarization degree of $\simeq 0.4\%$ (see [12]). A polarization level of $\simeq 2.5\%$ was measured by [32] with ISOPHOT at $170\,\mu$m for the nearby galaxy NGC 1808. A 99% confidence upper limit of 1.54% on the polarized emission of the ultraluminous infrared galaxy Arp 220 at $850\,\mu$m was reported by [31].

If polarization degrees of $\lesssim 2\%$ are typical for far-IR/sub–mm extragalactic sources, their contribution to polarization fluctuations in this wavelength region are likely sub-dominant compared to those due to Galactic dust, even at high Galactic latitudes.

subsubsectionThe Extragalactic Continuum Thermal Background

Thermal emission in the high frequency BPol bands is dominated by the same sources responsible for the Cosmic Infrared Background (Puget et al., 1996; Fixsen et al., 1998). The CIB sources are a large population of rapidly evolving far-IR luminous galaxies at moderate to high redshifts (z 1 — 3). The details of this population are not yet completely understood. However, upcoming projects, including Herschel, Planck and SCUBA2, will fill in much of the details that are now missing. By the time that BPol flies we will have a detailed understanding of the number counts and redshift distribution of the sources responsible for most of the CIB.

Frequency (GHz)	70	100	143	217	353
Beam FWHM	30'	20'	15'	10'	10'
Sensitivity (mJy, rms)	1	1.8	6.6	4.8	9
Confusion Limit		3mJy	3mJy	15mJy	50mJy

Table 2: BPol continuum sensitivity
Confusion limit estimates taken from Vaccari et al. (in preparation) and Rowan-Robinson et al. (in preparation).

3.2.1 Thermal Background and BPol

BPol will combine high continuum sensitivity with large beams (10' in the channels likely to be dominated by thermal emission). Point source flux sensitivity in each of the BPol beams are listed in Table 1, along with other relevant assumed parameters. The bright end of the far-IR source number counts are currently quite uncertain. Projects such as SASSy (the SCUBA2 All Sky Survey) will determine these to high precision in the coming years. However, the exquisite sensitivity of BPol combined with its large beams will ensure that continuum studies with BPol will be limited by confusion noise. Combining estimates of the 850μm (ie. 353 GHz) number counts from Rowan-Robinson et al. (in preparation) with the BPol beam sizes we find that the conventional confusion limit (1 source per 30 beams) arrives at a flux of 50mJy. This compares to BPol's expected rms sensitivity of 9mJy. The confusion noise will thus act as a major foreground contaminant for most of BPol's channels, and it will have to be detected and removed either internally, using component separation techniques, or externally through the use of ancillary data sets.

At this stage the only planned large area or all sky surveys at matching wavelengths to BPol are the SASSy 850μm survey using SCUBA2 and the Planck survey. SASSy will reach a 5σ flux limit of 150mJy, so does not get as deep as would be needed for BPol. Planck will reach a comparable sensitivity to the BPol confusion limit at 850μm but is factors of a few brighter than the BPol confusion limit at longer wavelengths. All these numbers are dependent on the final performance of Planck and SCUBA2. If Planck, for example, is able to perform four all sky surveys rather than the two that comprise the baseline mission, then its final sensitivities will approach the BPol confusion limits.

In the absence of appropriate all sky surveys at matching wavelengths we may instead extrapolate to longer wavelengths from other all sky studies. The most powerful here will be the IRAS, Akari and WISE surveys. All of these are at shorter far-IR or mid-IR wavelengths. However, it is likely that our knowledge of galaxy SEDs will be sufficient at the time BPol flies that we will be able to reliably extrapolate from these catalogs to the longer wavelengths needed for BPol.

3.2.2 Polarization Contribution

At the moment there are very few constraints on the polarization of far-IR luminous sources. There are rare examples (eg. 3c273, 3c279) where the far-IR emission is synchrotron dominated and where the polarization is consequently quite large. The majority of the far-IR sources that make up the CIB, though, are producing thermal emission from cool (30-50K) dust. The polarization contribution from this thermal emission is expected to be low unless there are strong magnetic fields in the emitting galaxy that lead to dust grain alignments. One of the few far-IR luminous galaxies whose polarization has been examined is Arp220, the nearest and archetypal Ultraluminous Infrared Galaxy. Seiffert et al. (2007) observed Arp220 at 850μm with the SCUBA polarimeter and have placed a 99% confidence upper limit of 1.54% on its polarization. SCUBA2 will also be equipped with a polarimeter. When it goes into operation we can expect more searches for polarization in far-IR luminous sources. At this stage, though, it would not appear that these sources will contribute a significant polarized flux to BPol.

S_{lim} (Jy)	average total polarization	Frequency channel (GHz)					
		44	70	100	143	217	353
0.1	$< p_r >= 0.05$	2.2e-3	3.6e-4	0.9e-4	3.5e-5	2.e-5	5e-5
0.1	$< p_r >= 0.028$	7.0e-4	1.0e-4	2.7e-5	1.0e-5	6.0e-6	1.6e-5
0.05	$< p_r >= 0.028$	3.7e-4	4.8e-5	1.3e-5	5.e-6	2.8e-6	0.7e-5
0.1	$< p_{IR} >= 0.01$	-	6.e-7	1.3e-6	4.e-6	2.e-5	5.e-4
0.1	IR+radio	7.0 e-4	1.0e-4	2.8e-5	1.4e-5	2.6e-5	5.e-4

Table 3: Estimated values of $\ell(\ell+1)C_\ell/(2\pi)$ (μK^2) due to undetected extragalactic point sources at the multipole $\ell = 100$, with $C_\ell \equiv C_\ell^Q = C_\ell^U = 1/2C_\ell^I < p_\nu^2 >$. The first three lines refer to radio selected sources whose contribution - for two different average polarization values, $< p_r >$ - has been calculated by adopting the number counts predicted by the evolution model of [9]. The fourth line refer to the possible contribution of undetected proto-spheroidal galaxies, by using the number counts of the model by [11]. In this latter case, due to the exponential decline of the number counts of proto-spheroidal galaxies above 10-30 mJy (at mm wavelengths) the choice of $S_{\rm lim} \geq 50$ mJy makes no difference in the estimated C_ℓ^Q values. Low-redshift far-IR sources are always giving a minor contribution to the total noise due to unresolved sources. In the last line we give our reference amplitude of the polarization power spectrum, C_ℓ, including the contributions of both radio and far-IR selected sources at $S < S_{\rm lim} = 0.1$ Jy.

3.3 Relevance at various multipole ranges

Given its very low instrumental noise and its very limited angular resolution, B-pol observations will be confusion limited at bright flux levels. If only directly detected sources are removed, the residual confusion noise will probably dominate over the CMB B-mode signal over a large range of angular scales (see e.g. [34]). To achieve the primary science goals it is then necessary to exploit additional, higher frequency data to go as deep as possible with the point source removal. High sensitivity, all-sky polarization sensitive measurements at 30, 44, 70, 100, 143, 217 and 353 GHz will be provided by the Planck satellite. According to the most up-to-date estimates [21] the best 5σ point source detection limits that can be achieved on Planck maps will probably be $S_{\rm lim} \sim 100$ mJy. A significant improvement can be obtained using prior knowledge of source positions, as shown by [41] in their analysis of WMAP data. The systematic 20 GHz survey, including polarization measurements, of the Southern sky, briefly described in § 3.1, is very important in this respect. The One Centimetre Radio Array (OCRA)*, currently in project, should carry out a survey of the Northern sky at 30 GHz.

Estimates of the Q or U power spectrum amplitude $\ell(\ell+1)C_\ell/(2\pi)$ (μK^2) due to Poisson distributed undetected extragalactic point sources at the multipole $\ell = 100$ are given in Table 3, for a few values of the detection limit and of the mean polarization degree. The strong clustering of high-z dusty galaxies detected by SCUBA and MAMBO surveys (see above) may substantially enhance fluctuations.

Clearly, a detailed understanding of the extragalactic point source contamination will be crucial to accurately measure the CMB B-mode polarization.

4 Future auxiliary observations

4.1 Future surveys of polarized diffuse components

It is clear from previous sections that a careful characterization of the polarized Galactic emission is necessary to detect the cosmic component of the B-mode. A cleaning of the foreground signal looks necessary even for the most optimistic T/S values ($T/S \sim 0.1$), unless observations

*http://www.jb.man.ac.uk/research/rflabs/OCRA-FARADAY.html

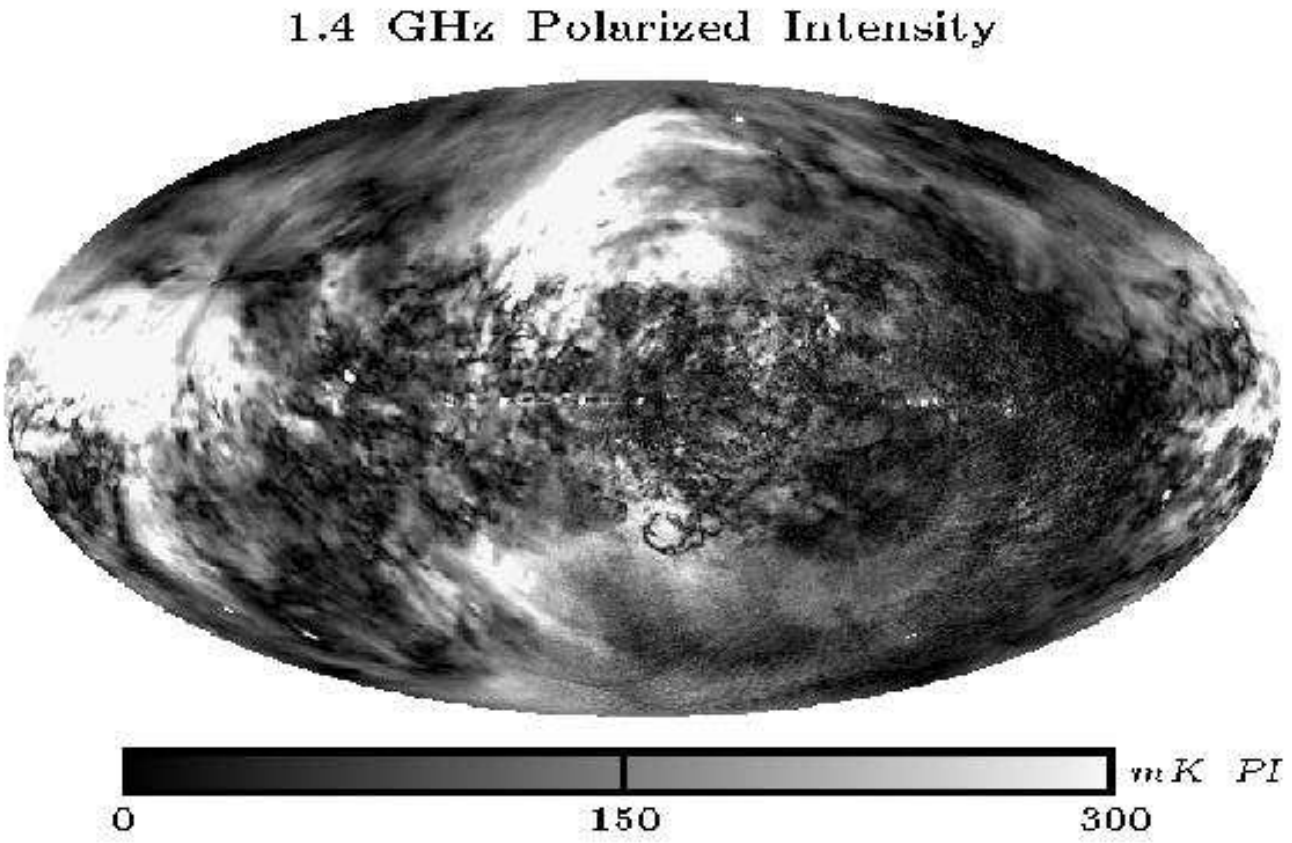

Figure 8: DRAO and Villa Elisa all-sky polarized survey at 1.4-GHz (from Reich 2006).

are carried out in selected lowest emission regions. Then, lower T/S values (some $T/S < 10^{-2}$) require to subtract the Galactic emission anywhere in the sky (see Sect. **??**).

The synchrotron emission data available so far include all-sky surveys both at 1.4 GHz (DRAO and Villa Elisa surveys – Wolleben et al. 2006, Testori et al. 2004) and 22.8 GHz (WMAP, Page et al. 2006) and a few small patches at high Galactic latitudes (Carretti et al. 2006 for a review). However, this data set does not yet look sufficient.

The 1.4 GHz data show strong depolarization in the Galactic disc up to $|b| = 30°$ and Faraday rotation effects are present at least up to $|b| = 50°$ (Figure 8). This is also supported by a multifrequency analysis using data from 0.4 throughout 1.4 GHz (Carretti et al. 2005).

The 22.8 GHz WMAP data have a frequency close to the optimal for CMB purposes, but the sensitivity is not yet sufficient. In fact, this map has low signal-to-noise ratio ($S/N < 3$) in some 55% of the sky on 2° angular scales (Figure 9), which corresponds to all the high Galactic latitudes, with the exception of strong local structures (e.g. Loop I).

Dedicated observations in small patches have allowed the only detection of the synchrotron signal in low emission regions at sufficiently high frequency. However, these cover only few tens of square degrees and larger surveys are necessary.

The knowledge about the polarized dust emission is even more scarse. Detections have been done on the Galactic plane by the Archeops experiment (353 GHz), but the signal is still elusive at high latitudes (Ponthieu et al. 2005).

Important steps are in progress to improve our knowledge about these CMB contaminant emissions.

The Parkes Galactic Meridian Survey (PGMS) is a project carried out at the Parkes telescope to survey a 5° wide strip centred on the Galactic meridian $l = 254°$ at 2.3-GHz. It covers all the Galactic latitudes from the Galactic plane down to the south pole with the goal to study the polarized diffuse emission behaviour as a function of the latitude. A first pass of the whole surveys is now complete, and it is expected to end in 2007 when the second pass of the last fields will be carried out. The survey's strip is positioned through one of the regions

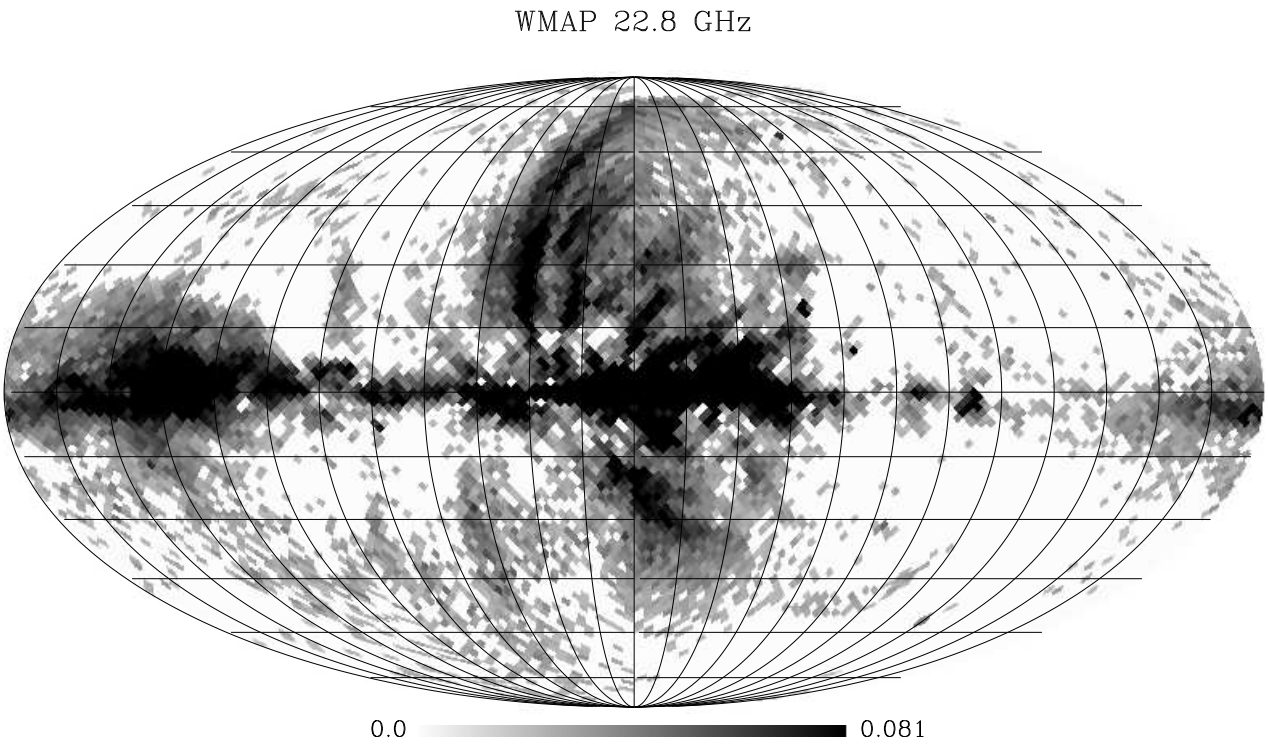

Figure 9: WMAP polarization map at 22.8-GHz with 2° pixels. All pixels with $S/N < 3$ have been blanked (white).

with lowest emission, so that PGMS can study the Galactic contribution sky areas promising for CMB B–mode detection. First results will be available soon.

The S-band Polarization All Sky Survey (S-PASS) will survey all the southern sky in temperature and polarization at 2.3 GHz. The project is on-going at the Parkes telescope (first run done in January 2007) and will be carried out in 2007-2009. The sensitivity of 1.5 mK rms on 9 arcmin beam will allow to detect the signal with $S/N > 3$ even in the lowest emission regions. When scaled to a 0.5° resolution, an $S/N > 10$ is expected so to allow a high precision charaterization necessary for the low CMB signal.

The C-band All-Sky Survey (C-BASS) will survey the whole sky in temperature and polarization at 5 GHz, with 0.85 degree beam and < 0.1 mK rms. The survey will be carried out from California and South Africa in 2008-2010, and will enter the public domain before 2012. Strenuous efforts are being made to minimize systematic errors such as stray light.

These three sky surveys at 1.4, 2.3, and 5 GHz available in few years represent a fundamental data set to characterize the polarized synchrotron emission.

Future polarization dust surveys: to be added

Besides ground-based observations, the Planck experiment will make available a set of nearly all-sky maps in a range between 30 and 850 GHz. This experiment will improve by a factor ~ 3 the sensitivities of WMAP at 30, 44 and 70 GHz. Althought this will not provide the same S/N ratio of the ground-based radio surveys (the 30 GHz map is expected to have about the same S/N of the 23 GHz map by WMAP, because of the weaker 30 GHz emission), this will significantly improve our knowledge of the synchrotron emission right in the frequency range of the CMB observations. About the polarized dust emission, instead, about almost nothing is known so far. Planck is thus expected to open a completely new window, detecting this component at least at the highest frequency channels.

4.2 Future polarization observations of extragalactic sources

Compact sources, either Galactic or extra-Galactic, are both a help and a hindrance to CMB experiments. Compact sources are of real use in refining an instrument's pointing model, confirming beam models, checking responsivity estimates, and measuring detector and electronics transfer functions. The sources used to do these tasks are obviously the brightest possible.

Unfortunately, not being at z=1000, most sources also contaminate CMB measurements. To this point, the most widely-used method used for removing the effects of point sources in CMB maps has been simply to mask them – that is, simply ignore data taken within a certain angular distance of sources. This will obviously be done for BPol to some extent as well. However, as discussed below, this will not be adequate for BPol.

4.2.1 Bright Sources

The brightest compact sources will be useful for such tasks as photometric calibration, characterizing the polarization properties of the experiment and reconstructing pointing. Given that the anticipated frequency bands for BPol are identical to, or a subset of, those of Planck, it can be assumed that *all* the brightest sources.

4.2.2 Faint Sources

WMAP detected about 60 sources at 100 GHz brighter than about 1 Jy [43]. At 100 GHz, BPol should have 1 μK sensitivity per 1' sky pixel, or roughly 0.03 μK sensitivity per 30'×30' beam. This equates to a point source sensitivity (assuming only Gaussian noise and ignoring foregrounds and other sources of noise) of about 1/2 mJy. Thus, BPol should detect sources roughly 2000 times fainter than WMAP, probably meaning well over 100000 sources (assuming $n \sim f^{-3/2}$).

By comparison, Planck is expected to have roughly 7 μK per 9.5'×9.5' beam, which equates to roughly 12 mJy point source sensitivity [44]. Thus, even with BPol's larger beams, it should detect sources roughly 20 times fainter than Planck, and as a consequence see roughly 100 times as many sources as Planck (assuming $n \sim f^{-3/2}$).

This means that any simple method of masking all detected sources, obviously, is inadequate for BPol, as one would end up masking a large fraction of the sky – it will be confusion limited. So BPol will have to live with extra-Galactic sources in the maps, and simply try to subtract the contribution of sources from the map, or from the power spectra measured. For this, additional surveys of sources will be valuable.

Here we list some upcoming *polarization* surveys which may aid BPol:

4.2.3 SPT

SPT had its first light on February 16, 2007 [45]. It has a 10 meter primary, providing 1' resolution at 2 mm with a field of view of one degree [46] and a thousand elements with NETs of 260 $\mu\mathrm{K}_{\mathrm{CMB}}\sqrt{\mathrm{s}}$. An unpolarized survey of 4000 square degrees is planned, and a proposal for a polarization-sensitive instrument with similar capabilities has been made [47].

4.3 SCUBA2

SCUBA2 is a new bolometric camera which will be installed at the JCMT beginning in mid-2007 and reaching its full performance in mid-2008. It is the successor to SCUBA and will boast significant improvements in both raw sensitivity and in survey capabilities. SCUBA2 will provide simultaneous diffraction limited imaging at 850 and 450 μm ($\sim$ 14" and 8" FWHM respectively), with a field of view of 7'×7'. A polarimeter will be available for use with SCUBA2 to produce

imaging polarimetry or to conduct polarisation surveys. Polarisation surveys in some star formation regions (eg. Gould's Belt) are already planned as part of the SCUBA2 Legacy Surveys (see, for example, `http://www.jach.hawaii.edu/JCMT/surveys/SurveyAllocations.html`).

4.3.1 ALMA

The Atacama Large Millimeter Array (ALMA) will be one of the largest ground-based astronomy projects of the next decade, is a major new facility for world astronomy. ALMA will be comprised of a giant array of 12-m submillimetre quality antennas, with baselines of several kilometres. An additional, compact array of 7-m and 12-m antennas is also foreseen. Construction of ALMA started in 2003 and will be completed in 2010. The ALMA project is an international collaboration between Europe, Japan and North America in cooperation with the Republic of Chile. It will have some polarization capabilities, and thus can provide detailed information about individual sources in the BPol bands.

4.3.2 POLKA

The "Polarimeter für Bolometer-Kameras" is a new tunable polarimeter for mm and submm wavelengths. Very low insertion losses and the possibility to tune its opearating wavelength in a wide range makes it a versatile instrument. It will be used with the MPIfR bolometer arrays at different wavelenghts (2, 1.2, 0.87 mm) to produce high-resolution maps of polarization.

4.3.3 HERTZ

4.3.4 IRAM

5 Non-Gaussianities in polarization

The standard inflationary scenario predicts that both the temperature and polarization anisotropies of the CMB are statistically isotropic and Gaussian distributed. A large number of works have already been performed to test the statistical distribution and isotropy of the CMB temperature maps, specially for the WMAP data. Several anomalies have already been found like North-South assymmetries [89], low-multipole alignments [86, 88], phase correlations [85], the cold spot [92, 87], alignment of CMB structures [93]. Whereas the origin of some of those anomalies can be assigned to foreground residuals or systematics, for others an intrinsic origin cannot be discarded. For polarization the situation is completely unknown since no statistical study has been performed yet due to the lack of good quality maps. It is clear, however, that the statistical distribution of CMB polarization is crucial to discriminate among several possibilities to interpret those anomalies. On the other hand, non-standard scenarios in the early universe make specific predictions for both temperature and polarization distributions. In particular, constraints already imposed on some scenarios based on temperature alone can be significantly improved. For instance, the constraints on the non-linear coupling parameter f_{NL} can be reduced by a factor of 2 if polarization is included in the analysis in addition to temperature [84].

The statistical study of CMB polarization represents a very difficult task for several reasons. First, the Galactic foregrounds are expected to be relatively more prominent in polarization. Therefore it is crucial to know them with good accuracy in order to be removed at a very high precission. Second, for small enough values of the tensor-to-scalar parameter, $r \lesssim 10^{-3}$, the background of extragalactic sources (below 1 Jy in intensity) as well as the lensing induced B-mode dominate over the primordial B-mode signal $\ell \gtrsim 10$ [91]. The polarization effects of these two extragalactic foregrounds should be significantly decreased in order to unveil the cosmological signal at those levels of sensitivity. Another problem is the presence of masks in the maps (due to either non-observed regions of the sky or the impossibility of a good foreground

removal) which produce a certain amount of mixing of E and B-modes depending on the area and geometry of the masked regions. Furthermore the systematics in polarization experiments are expected to be much more relevant and complex than in intensity ones. In this respect statistical studies can be very beneficial to test the presence of systematics and/or foreground residuals in the polarization maps.

5.1 Non-Gaussianity from diffuse foregrounds

5.2 Non-Gaussianity from point sources

Up to date, there are not works on the literature dealing with the point source impact on the CMB Gaussianity on polarization. However, some hints could be deduced by extrapolating some known results from temperature.

Whereas for the CMB E-component —assuming that the brightest point sources (e.g. above 1 Jy in temperature @ 100 GHz) are removed (with negligible errors) from the Q and U maps— the point source emission is not a major problem for an experiment with an angular resolution of around 20 arcmin, the situation for the CMB B-component could be much worse. For instance, for scalar-to-tensor ratio $r \sim 10^{-3}$ the extragalactic sources will dominate at intermediate and small scales ($\ell \geq 10$, [91]).

The situation could be much more propitious if fainter sources were eliminated. However, as our current experience from temperature analyses is showing, in many cases it is more convenient to mask faint sources rather than removing them, since typical erros induced by point source removal are important and very difficult to simulate (with the typical accuracy required by non-Gaussian analyses). Of course, there is a limit in the amount of sources that could be masked, since the most we cut, the largest are the errors induced in the E and B components. However, a proper analysis of the optimal masking is lacking and some steps on this direction should be done.

Despite the mask flux limit, the non-Gaussianity induced by the background of remaining point sources might be still important for the CMB B-component. An approach similar to the one followed in temperature, assuming general behaviors for the different point source populations, can be adopted to deal with this contamination. The key point is to define the pattern followed by a given non-Gaussian statistic due to a point source population. This methodology has been used with the bispectrum [90, 82] and the skewness and kurtosis of the Mexican Hat Wavelet coefficients [83], and can be easily extended to other statistics. Of course, this approach relies on our knowledge about the different microwave point source populations (for instance, obtained from data like the one expected from Planck) and, therefore, methods requiring general information (like a parametrized law) are much more useful than others needing more specific details.

6 Methods to deal with diffuse components

6.1 Non-blind methods

6.2 Blind component separation methods

The Independent Component Analysis relies on the statistical independence of the superposition of different astrophysical emissions, as well as on their different scaling behavior in frequency [Amari and Chichocki(1998)]. By linearly combining the signals at different frequencies, the maxima of the neg-entropy are found, and correspond to the independent components which are mixed in the data. The ICA procedure has been introduced in CMB measurements for the first time by [Baccigalupi et al.(2000)]. The FastICA, a computationally fast implementation of the ICA concept [Hyvarinen and Oja(1999)], has been applied later to the

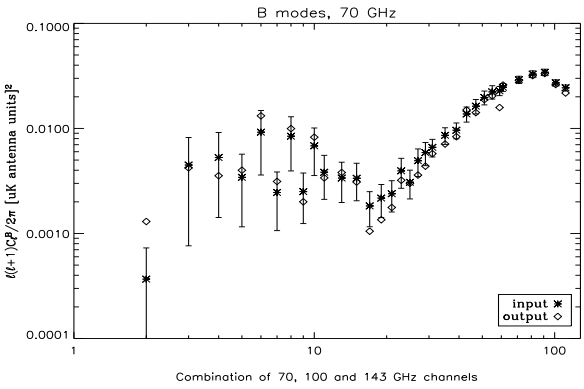

Figure 10: The input CMB signal for B modes (asteriscs) with cosmic variance errorbars, and the reconstructed one (empty squares).

simulated data of the Planck satellite in total intensity [Maino et al.(2002)] and polarization [Baccigalupi et al.(2004)]. It has been applied also to the data from real experiments, namely COBE [Maino et al.(2003)], BEAST [Donzelli et al.(2006)] and WMAP [Maino et al.(2007)]. In the latter work, the main results of the analysis were the reconstruction of the first acoustic peak as well as the north-south asymmetry in the data, in agreement with the WMAP results [Hinshaw et al.(2007)]. Finally, [Stivoli et al.(2006)] performed a parallelization of the FastICA code, applying it to simulated data in polarization for the extraction of the B modes from a patch in the sky, being able to conduct Monte Carlo simulation and quantifying the precision of the reconstruction to be comparable with the uncertainty from cosmic variance and instrumental noise.

6.2.1 First applications to Bpol

In figure 10 we show the results of our first application of the FastICA procedure to the Bpol data. The frequency channels that we consider are 70, 100 and 143 GHz with sensitivities given by 3 μK thermodynamic on squared pixels with 1 arcminute side; before processing, all channels were degraded to a commmon angular resolution corresponding to FWHM=2 degrees. The data are a mixture of CMB, thermal dust and synchrotron emissions, built as follows. The CMB corresponds to a cosmological concordance model with $T/S = 10^{-3}$. The total intensity templates for synchrotron [Haslam et al.(1982)] and dust [Finkbeiner et al.(1999)] are multiplied by a parameter representing the polarization fraction, p_{dust} and $p_{synchrotron}$, which are assumed to be constant. The resulting polarized intensity is then multiplied by synthetic maps of $\sin\theta$ and $\cos\theta$, where θ represents the polarization angle, in order to get templates for Q and U. The latter maps were obtained with the `synfast` procedure in HEALPix, starting from power spectrum $C_l^{\sin\theta} = C_l^{\cos\theta} \propto l^{\beta_{signal}}$, where *signal* stays for dust or synchrotron. The parameters p_{signal} and β_{signal} are then adjusted to match the WMAP measurements; $p_{dust} = 11\%$, $p_{synchrotron} = 10\%$, $\beta_{dust} = \beta_s ynchrotron = -3.2$ provide a satisfactory agreement. In the figure we plot the result of the input versus output CMB power spectrum for B modes, and the error bars corresponding to the cosmic variance plus instrumental noise. Apart from a few points, the reconstruction is within cosmic variance for all relevant multipoles. The configuration with a frequency channel which is lower with respect to the foreground minimum at 70 GHz yields a better control of the synchrotron emission, represented as a distribution of the reconstructed power spectrum which is close to be Gaussian distributed around the signal from the input sky. Empirical runs, not shown here, indicate that a suitable choice for the low frequency channel should be not too far from the foreground minimum at 70 GHz, with sensitivity comparable with the other cases.

6.3 The phase method

According to the standard cosmological model, fluctuations in both temperature and polarization should be statistical homogeneous, Gaussian, and with each mode of the resulting spherical harmonic expansion having a random phase. Any correlations in the phase between Fourier modes is consequently a diagnostic of non-Gaussianity or non-stationarity (Coles et al. 2004). Furthermore, the phases of *cleaned* sky maps should be independent of the various foreground templates, leading to methods of foreground removal that improve upon the standard "minimum variance" approach and which may be more robust to the presence of localized foreground features. In the following we discuss a couple of recent examples of this approach.

Chiang et al. (2007) used a compressed (one-dimensional) representation of the spherical harmonic coefficients for each l mode, using the WMAP DILC maps. Based on the a priori assumption that the CMB signal should be statistically independent of, and consequently have no significant correlation with, any foregrounds, they cross-correlated the $12 \leq lleq10$ modes, which are claimed by the WMAP team to be free of contamination and suitable for whole sky analysis, finding that 8 out of the 9 modes are negatively cross correlated with the foreground maps, an event which has a probability of only $9/512 \sim 0.0176$ for truly uncorrelated signals. Furthermore, the local extrema of the 1DFR curves between the DILC and those of the foregrounds for l=2 and 6 are correlated with significance level below 0.04. They also discussed the minimum variance optimization method and use the properties of the measured cross-correlation to estimate the possible level of contamination present in the DILC map.

Chiang, Naselsy and Coles (2007) tested the de-biased internal linear combination (DILC) map produced from the 3-year WMAP data. The phases of the modes $l = 3$ and $l = 6$ of the CMB maps cross-correlate with the foregrounds, suggesting the presence of residual contamination in the DLC map even on these large scales. There is also a strongly significant alignment with the Galactic meridian which, together with the cross-correlation of DILC phases with the foreground maps, strongly suggests that even the lowest spherical harmonic modes in the map are significantly contaminated with foreground radiation.

So far the applications of phase analysis have been largely restricted to temperature, but the generalization of the approach to polarization studies is conceptually straightforward. The strong evidence of residual contamination in the supposedly clean WMAP DILC suggests that cleaning the polarization maps will be a considerable challenge and that such sensitive diagnostics of residual artifacts will be required.

6.4 "Hybrid" methods

6.4.1 Correlated Component Analysis for Bpol

The benefit and the peculiarity to measure the CMB emission from a satellite is the possibility to be sensitive to the large scale. In this case we have to take care of foregrounds and mainly the galactic diffuse foregrounds. A better knowledge of foregrounds contamination will be the key factor to improve our knowledge about CMB; in fact the foreground contamination is estimated to be the main non-systematic sources of contamination for a CMB map (Ponthieu et al).

As explained in previous section there are several galactic and extragalactic emissions in the range of frequency detection of CMB. One of the main task of data analysis is to separate the CMB signal from the sum of all these incoming radiations. We will review the CCA approach (Correlated Component Analysis).

The Correlated Component Analysis (CCA, Bedini et al.) exploits information on the second-order statistics to estimate the spectral behavior of the astrophysical components. As usual, we express the data vector $\mathbf{x}$ as:

$$\mathbf{x} = \mathbf{H}\mathbf{s} + \mathbf{n} \tag{1}$$

where $\mathbf{H}$ is a $M \times N$ mixing matrix, $\mathbf{s}$ is the N-vector of sources and $\mathbf{n}$ the M-vector of instrumental noise. The generic element h_{dc} of the mixing matrix is proportional to the spectrum of the c-th source at an effective frequency within the d-th sensor passband. Using eq. (1) we implicitly assume that the spatial pattern of the physical processes is independent of frequency and that the effects of the telescope beam has been equalized in all channels.

The aim of CCA analysis is to find the best set of parameters for the mixing matrix given a model that represent our believes regarding the scaling of components. We developed also several test that allow us to understand if our model is a consistent representation of the physical mechanisms.

The recovered informations can be used as an input for traditional non-blind methods, as MEM, or other Bayesian inversion techniques, to perform source separation.

In this sense The CCA algorithm is a semi blind or "hybrid"code: the mixing matrix A is parametrized in a suitable manner an then the value of the parameters are founded minimizing a quantity related with the covariance matrix. After that we need to recover the estimated sources components performing a wiener filter or a MEM based inversion. We can decide case by case if we need to introduce priors in the inversion or not. We will briefly discuss some details of the CCA implementation.

Given a generic signal $\mathbf{X}$, defined in a two dimensional space with coordinates (ξ, η), the covariance matrix of this signal is:

$$\mathbf{C}_X(\tau, \psi) = \langle [\mathbf{X}(\tau, \psi) - \mu][\mathbf{X}(\xi + \tau, \eta + \psi) - \mu]^T \rangle \tag{2}$$

where $\langle ... \rangle$ denotes expectation under the appropriate joint probability, μ is the mean vector and the superscript T means transposition. Every covariance matrix is characterized by the shift pair (τ, ψ), where τ and ψ are increments in the ξ and η coordinates.

From eq. (1) we can easily derive a relation between the data covariance matrix $\mathbf{C}_x$ at a certain lag, the source covariance matrix $\mathbf{C}_s$ at the same lag, the mixing matrix $\mathbf{H}$, and the noise covariance matrix $\mathbf{C}_n$:

$$\mathbf{C}_x(\tau, \psi) = \mathbf{H}\mathbf{C}_s(\tau, \psi)\mathbf{H}^T + \mathbf{C}_n(\tau, \psi). \tag{3}$$

The covariance matrix $\mathbf{C}_x$ can be estimated from the data with:

$$\hat{\mathbf{C}}_x(\tau, \psi) = \frac{1}{N_p} \sum_{\xi,\eta} [\mathbf{x}(\xi, \eta) - \mu_x][\mathbf{x}(\xi + \tau, \eta + \phi) - \mu_x]^T \tag{4}$$

where N_p is the number of pixels sampling the data. Given a noise process, we can model the noise correlation matrix $\mathbf{C}_n$: for example, if noise can be assumed signal-independent, white and zero-mean, for $(\tau, \psi) = (0, 0)$ $\mathbf{C}_n$ is a diagonal matrix whose elements are the noise variances in the measured channels, for $(\tau, \psi) \neq (0, 0)$ $\mathbf{C}_n$ is the null $M \times M$ matrix. Anyway, if the noise process is expected to deviate significantly from this ideal model, $\mathbf{C}_n$ can be computed using noise maps in the same way we did for $\mathbf{C}_x$.

Once $\mathbf{C}_x$ and $\mathbf{C}_n$ are known, eq. (3) can be used to identify the mixing operator $\mathbf{H}$. The strategy of CCA is to parameterize the mixing matrix to reduce the number of unknowns and to take into account enough nonzero shift pairs (τ, ψ) to estimate both $\mathbf{H}$ and $\mathbf{C}_s$.

To solve the identification problem we perform a minimization over:

$$(\Gamma, \Sigma(:,:)) = min \sum_{\tau,\psi} \parallel \mathbf{H}(\Gamma)\mathbf{C}_s[\Sigma(\tau, \psi)]\mathbf{H}^T(\Gamma) + \\ -\hat{\mathbf{C}}_x(\tau, \psi) - \mathbf{C}_n(\tau, \psi) \parallel \tag{5}$$

where Γ is the vector of all parameters defining $\mathbf{H}$ and $\Sigma(:,:)$ is the vector containing all the unknown elements of matrices $\mathbf{C}_s$ for every shift pair.

The main product of CCA is then an estimate of the mixing matrix $\mathbf{H}$; exploiting the scaling ambiguity of the problem, we estimate a normalized mixing matrix, obtained by assigning value 1 to all the elements of an arbitrarily chosen row.

This method was intensively tested for Temperature dataset (Bonaldi et al.). The CCA algorithm showed an effective foreground subtraction, with residual uncertainties inducing a minor contribution to errors on the recovered CMB power spectrum. This test demonstrate that CCA method, applied to simulated data (with Planck specifications), is a promising tool to estimate the mixing matrix parametrizing the frequency scaling of different astrophysical signal in CMB observations. Exploiting non-optimized component separation techniques, such as Wiener Filter and pseudo-inverse filter, such errors allow us to estimate the CMB power spectrum with an uncertainty of the order of 1% on the angular scales constrained by our patch size.

We are working also with real data performing a component separation using WMAP data (paper in preparation).

We will perform an analogous test for polarization analysis. In principal the estimation of the mixing matrix can be performed separately for Q and U maps exactly as for a Temperature map (pixel based method). The problem is more delicate in the inversion step. In fact all the harmonic methods require to perform a deconvolution with the beam. Therefore we will need to develop an inversion technique that will take care of both Q and U simultaneously.

7 Point source removal and background estimation

Unfortunately, many of the component separation techniques that are generally used to separate diffuse Galactic foregrounds are not well suited to deal with point sources. This is mainly due to the fact that each galaxy is an independent source, different, in principle, to any other source in the sky. Albeit average energy spectra can be defined for different source populations, the spectral emission law is different for each galaxy and it makes inefficient to apply separation methods which exploits a single energy spectrum for this foreground component.

If the lack of knowledge on their spectral emission properties can be troublesome, their projected angular shape is basically the same for all of them: a Dirac's δ-like response convolved with the instrument beam response function. Thus, techniques that take into account the specific angular shape of point sources, such as wavelets and bandpass filters, are particularly useful for detecting them. In the last few years a number of techniques have been proposed for the specific case of point-source detection in CMB maps, but the matched filter (MF) [42] and the Mexican Hat Wavelet Family (MHWF) [38] have been the most successfully applied.

From the analysis of the first three years survey data the WMAP team has obtained a catalogue of 323 extragalactic point sources (EPS; [39]) by filtering in the harmonic space by the global MF. The fact that almost all sources detected by WMAP were previously catalogued at lower frequencies suggests that a fuller exploitation of the WMAP data can be achieved complementing the *blind* search already carried out by the WMAP team with a search for WMAP counterparts to sources detected at lower frequencies. The latter approach exploits the knowledge of source positions to extract as much information as possible on their fluxes.

The NEWPS (New Extragalactic WMAP PS) Catalogue [41] have been built following the *non-blind* philosophy: projection of hundreds of flat sky patches centered in the positions of the brightest sources at 5 GHz in the WMAP maps, and then analyze them using the MHW2. The results were 100 "new sources" (5σ sources not present in the WMAP catalogue) and hundreds of 3σ flux estimations.

Before the lunch of the Bpol Satellite the Planck PS Final Catalogue will be available and, as the sensitivity of Bpol will be better than Planck's one but not its angular resolution (in this case is not expected to detect a significant fraction of new sources not seen by Planck),

to apply a *non-blind* will be very appropriate for the problem of PS removal. Moreover, the same technique used to build NEWPS has being used to study the polarization properties of the PS directly in the WMAP polarized maps. Very preliminary results show that more than 20 sources could be detectable with a signal to noise greater than 5 (several tens if a 3σ level is allowed).

Another important problem related with the EPS contamination is the estimation of the background level produced by the undetected point sources: even knowing the completeness level of our PS catalogue and using very accurate models for the source populations, some degree of uncertainty is introduced due to errors in the flux estimation of the faintest sources (also called Eddintong bias) or due to the fact that some sources are already detected below the completeness level, etc.

A couple of methods that can be used to obtain a direct estimation of the background level caused by the point sources have been published in the last years. Both methods are based on the strong Non-Gaussianity signal produced by the point sources.

[40] directly determined in the WMAP maps the power-spectrum generated by the residual sources using a relation between the measured point source bispectrum and their power-spectrum as a function of the flux limit, without relying on any extrapolations.

On the other hand, [37], by filtering CMB maps with the first members of the MHWF, enhanced the non-Gaussianity due to undetected point sources to determine their third and fourth order cumulants till relatively low fluxes limits. From these cumulants, they also determined the parameters that define the underlying source number counts assuming a power law.

Finally, it is important to point out that all the techniques discussed in this section will be deeply tested with the future Planck mission data, allowing us to a better understanding of the point source properties in total intensity as well as in polarization.

8 Exploiting foreground physical modelling

8.1 The Galaxy

8.2 External galaxies

Polarized synchrotron radiation is a signature of ordered magnetic fields. Although the physical mechanism of this nonthermal emission is the same in different types of galaxies (from normal to active), the size of the emitting region, the physical conditions and the energy output vary substantially. To perform a physical modeling of polarized foreground sources, one needs to define (1) the type of a galaxy, (2) the physical model of polarized emission, and (3) its evolution with the cosmological epoch.

8.2.1 Normal spiral galaxies

With a flux density limit 100 mJy per beam of BPOL at frequences between 70-300 GHz, the main populations of foreground sources will be relatively bright star-forming galaxies and active galactic nuclei (AGN). The former population consists of late-type spiral and starburst galaxies. There is observational evidence of significant polarized emission (1-10is a signature of large-scale regular magnetic fields, or of compressed or sheared turbulent fields. Little is known about the importance of compression and shear in young starburst galaxies. Regular fields can be modeled by the dynamo mechanism which is capable to order magnetic fields on scales of tens of kiloparsecs during the lifetime of a galaxy. An evolutionary model of regular magnetic fields in normal spiral and in starburst galaxies is in progress. This will allow the simulation of the population of polarized normal galaxies and their number counts. Their contribution to the polarized foreground is expected to be small because they are intrinsically faint sources and

their surface density is small at radio-mm frequences which leads the lack of normal disk galaxies in the existing deep but small sky-coverage polarization surveys. Furthermore, the degree of polarization is expected to decrease with distance of the galaxy due to depolarization within the beam. Even if net polarization remains for a single unresolved galaxy, a number of galaxies within the beam will have random mean polarization angles so that their polarized emission mostly cancels. Models based on polarization data of nearby galaxies are in preparation.

8.2.2 Starburst galaxies

Until recently very little was known about the polarization properties of starburst galaxies. New deep (340 microJy) polarimetric observations of the ELAIS-N1 region at 1.4 GHz identified most sources with active galactic nuclei (AGN) hosted by dusty elliptical galaxies and with few AGN having extended radio structure, but none of polarized sources is associated with an active star-forming galaxy (Taylor et al., submitted). The spectral energy distribution of starburst galaxies between 1 and 300 GHz is due to synchrotron (steep power law) and thermal radiation (from few tens of GHz and higher). The absence of polarization at 1.4 GHz effectively rules out also existence of significant polarized emission at high frequencies 300 GHz. We may preliminarily conclude that starburst galaxies will have insignificant contribution to the foreground of polarized sources seen with B-POL.

8.2.3 Radio-loud AGN

The source of polarized emission in radio-loud, flat-spectrum galaxies, quasars and BL Lac objects is associated with powerful jets indicating the presence of ordered magnetic fields in optically thin synchrotron- emitting regions. For all three classes of objects the fractional polarization of the cores of the jets at 15 GHz is generally less than 5fractional polarizations (¿501389). Due to relativistic boosting of radiation and flat/inverted spectra radio-loud AGN will be detected at high redshifts and radio-to-submm frequencies. At high radio frequencies (¿15 GHz) the bulk of synchrotron emission is radiated from the innermost part of the jet (core) in which the magnetic fields are found to be well-ordered and oriented along the jet, and hence, it is expected that the synchrotron emission of radio-loud AGN will be more polarized with increasing frequency. Observations of polarized emission support this scenario, although depolarization also can play a role (Ricci et al. 2004; A&A 415, 549). Although the fraction of luminous radio-loud AGN sources is not large (10polarized foreground is expected to be significant because of the relatively high flux density detection limit of BPOL (100 mJy per beam).

8.2.4 Radio-quiet AGN

Tucci et al. (2004 MNRAS 349 1267) reported that 90sources selected from the NVSS-GB surveys are steep-spectrum ones. Moreover, they found that faint steep-spectrum radio sources are more polarized than the strong source population (see also Messa et al. 2002; AA 396 563). This trend was confirmed for fainter sources (340 microJy; Taylor et al., submitted) which were identified with galaxies having faint PAH emission and an old stellar population - both indicative that the polarized emission is associated with AGN activity. The median fractional polarization increases to 6density between 1 and 30 mJy (Taylor et al.). These sources are most probably steep-spectrum, radio-quiet AGN. They are too faint to be detected by BPOL, but they will significantly contaminate the polarized foreground of deep surveys. Polarization of steep-spectrum AGN increases with frequency and it is high or comparable (median 4.8on a common mechanism of jet production in radio-loud and radio-quiet AGN. The luminosity of the latter is weaker by two orders of magnitude at 70 GHz and comparable at 300 GHz. They comprises 90and their contribution to the polarized foreground seen with BPOL is expected to be significant.

8.2.5 Physical modeling of jets

Physical models of the jet, which incorporates the velocity field and magnetic field structure of the jet, have been successfully fitted to observational data (see for example, Laing et al. 2006; MNRAS 372, 510) only for few radio-loud AGNs so far. The origin and evolution of the jet is closely related to the evolution of the central engine, i.e. the accretion disk - black hole system, which in turn is linked to the evolution of the whole galaxy. There are many unresolved problems such as the accretion mechanism, the jet triggering mechanism, the duty circle of jet activity, the importance of the magnetic fields, and the mass/spin of the black hole in jet production. It is not clear yet whether the same physical mechanism is responsible for generation of jets in radio-loud and radio-quiet AGN.

To our knowledge the physical modeling of the evolution of jets has not yet been performed because of complexity of physical processes acting in the central engine. A recent attempt for grand unification of AGN (see for example, Cen, astro-ph/0702660) shows the complexity of the problem and number of assumptions involved (no evolution is considered!). Physical modelling of the polarized energy output of AGN and its evolution would be an even more challenging task which is, practically, not feasible in the light of present knowledge.

9 Residual contamination in CMB maps

9.1 Residual errors from diffuse component separation

9.2 Residual errors from point source removal

Although, currently, there is a lack of direct information about the performance of point source detection and estimation techniques on Q and U maps, some estimation on the residual errors induced on the polarized CMB maps can be inferred from their application to temperature maps.

In principle, there are two possible sources of residual errors arisen from point source removal: 1) inaccurate determination of the point source location and 2) error in the flux estimation. The former is less important than the later since, more likely, point source detection on polarized maps will be not blind, i.e. ancillary data (in the form of already known point source catalogues) will be used to identify the point source positions. A similar approach was recently followed on WMAP temperature data [94] with very successful results. For the point source detection on Bpol, the final extragalactic source catalogues obtained from Planck would be, undoubtedly, very useful to identify the positions of the point sources. Regarding the error on the flux estimation, again, we can just extrapolate our knowledge from temperature analysis. According to [94], errors on the flux estimation are ≈ 260 mJy at 60 GHz (FWHM ≈ 20 arcmin). This limit is imposed by the CMB and the Galactic and extragalactic backgrounds rather than the instrumental noise. Hence, a very rough estimation, indicates that typical errors on the estimation of the point source amplitude on Q and U maps are expected to be of $\sim 20 - 40$ mJy at 70 GHz. To achieve this error level is crutial to have a very detailed knowledge of the beam shapes.

9.3 Implications for the CMB

9.3.1 Residual errors at low multipoles ($\ell \lesssim$ few tens)

9.3.2 Residual errors at intermediate multipoles (few tens $\lesssim \ell \lesssim$ few hundreds)

The intermediate multipole region (l ranging from tens to hundredths) is important for the B-mode angular spectrum of CMB basically for two reasons, i.e., because it is rather independent of the reionization optical depth τ and more than 50% of the power is expected to reside there.

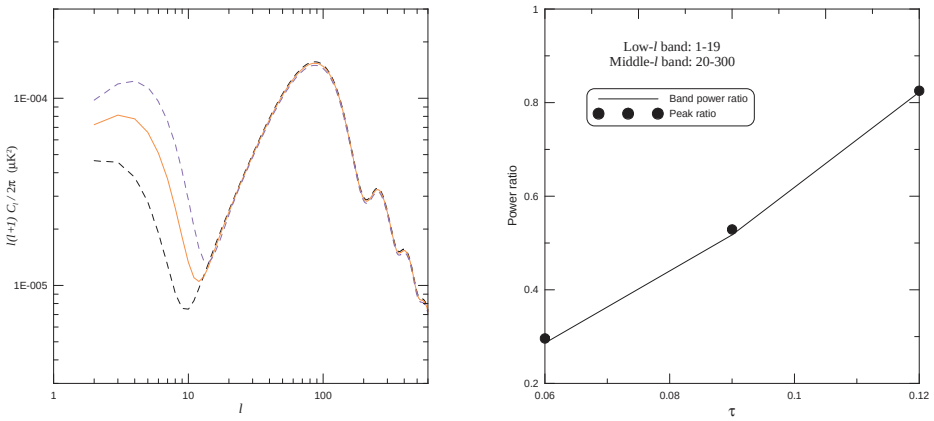

Figure 11: Left panel: The CMB B-mode angular spectra for reionization optical depths $\tau = 0.06, 0.09$ and 0.12. The tensor-to-scalar ratio is assumed to be $r = 10^{-3}$. Right panel: The ratios of the low-l to the middle-l band power (full line), and of the peak values in the same bands (filled circles).

Figure 11 reports the the CMB power spectra for the standard set of cosmological parameters as in the WMAP data set for the "lcdm+tens" model [76], but for $\tau = 0.06$, 0.09 and 0.12. Clearly the spectrum is strongly affected for $l < 20$, with variations by a factor ~ 3, but differences cannot be appreciated at higher l. The main peak is firmly located (if any other parameters are fixed) at $l \approx 85$. The right-hand panel of Fig. 11 reports the ratio of band powers in the 2-19 and 20-300 bands as a function of τ; for reionization histories favored by the 3-year WMAP release (differing from the 1-year release) this ratio is definitely less than unit, and for the above 3 values of τ lies in the range 0.3-0.8. The cosmic variance for the band power $P = \sum_l (2l+1)C_l$ is

$$\mathrm{var}(P) = 2\sum_l (2l+1)C_l^2 \tag{6}$$

(full-sky estimate for the ideal case of no detector beamwith limits). Thus the power fluctuation $[\mathrm{var}(P)]^{1/2}$ in the flat band approximation amounts to about 15% and 1% of the power in the above two bands, respectively. Since the uncertainties on other cosmological parameters are expected to have smaller effects than the uncertainty on τ, we can conclude that (i) the total power has a rather well defined relationship with the GW background (i.e., with the parameter r), and (b) the band power ratio can be very useful for a consistency check of the cosmological scenario. It is therefore important that angular resolution can allow to recover the intermediate scale information, also in frequency channels where the CMB signal is completely masked by foregrounds and sky maps can only be useful to characterize the foregrounds themselves.

Even in this lucky region the knowledge of foregrounds must be pushed well beyond the present-day knowledge. For estimates of the accuracy of a BPol detection of the angular spectrum, however, foregrounds can be modelled in accordance to WMAP results. Waiting for a comparative analysis of advanced foreground-subtraction methods, a simple treatment can be given by the approach of [91], updated by the use of WMAP results. This approach assumes that for each Galactic foreground the best template is essentially determined at one

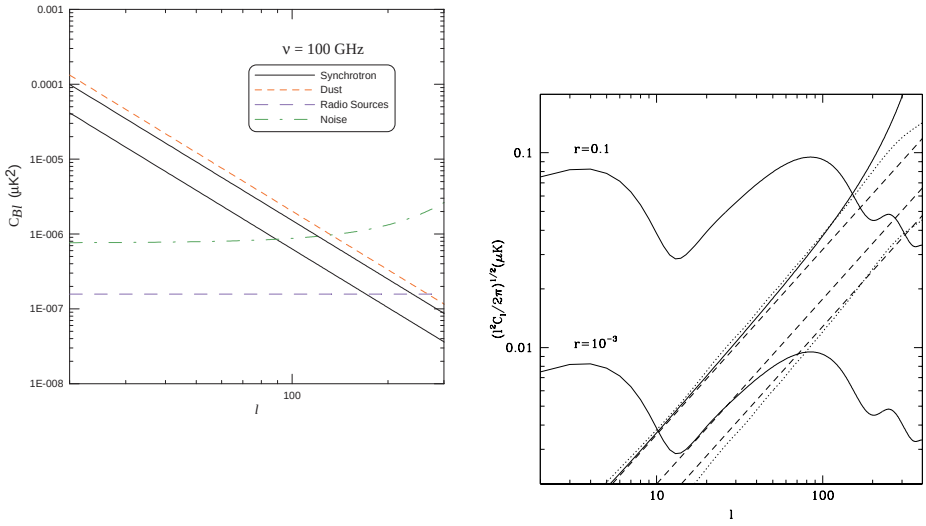

Figure 12: Left panel: B-mode angular power spectra of Galactic and extragalactic backgrounds at 100 GHz . Two syncrotron curves correspond to $C_{Bl} = 0.10l^{-2.6}$ and $0.24l^{-2.6}$ μK^2 respectively, obtained by extrapolations with $\beta_{synch} = -3.1$ and -2.8. The dust curve is normalized according to model 8 of ref. [79]. The radio source spectrum is contributed by sources with $S < 300$ mJy. The noise level is computed for a 0.5° beam. Right panel: The 100 GHz angular spectra of radio sources (dashed lines) and lensing (dotted), compared to noise (full line). The radio source spectra are given for limiting fluxes of 1 Jy, 300 mJy and 150 mJy. The lensing spectra are given before and after a redution to 10%.

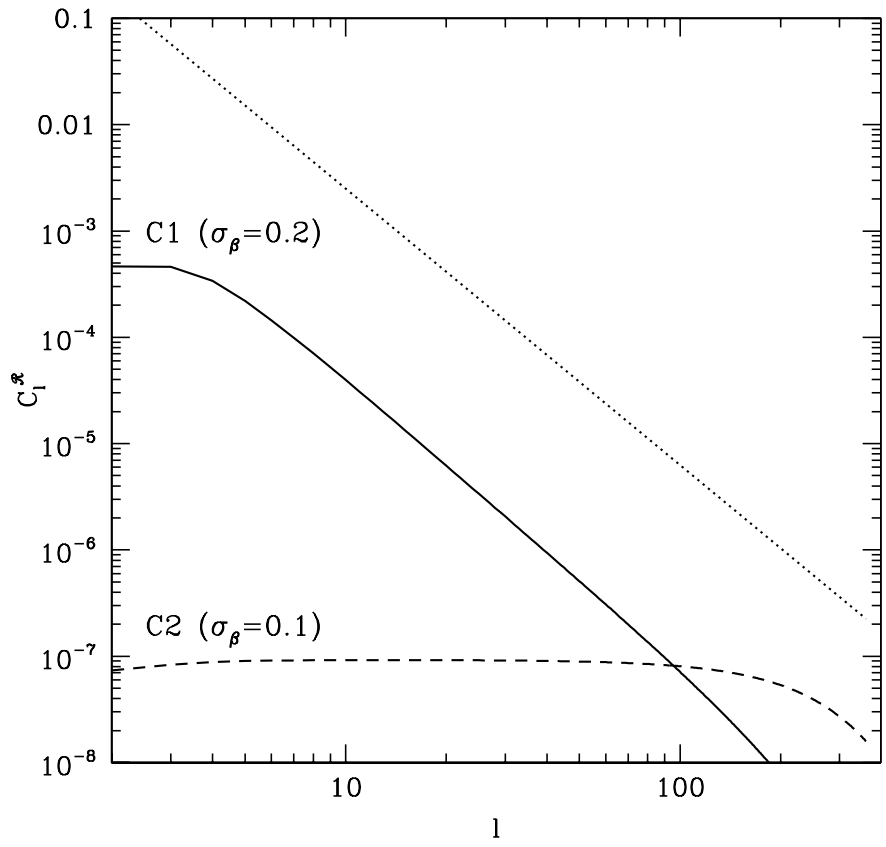

Figure 13: The $C_l^{R_1}$ contribution to the residual C_{Bl}^{fore} of Galactic backgrounds. The curves should be multiplied by $[\ln(\nu_t/\nu_o)]^2$. Cases C1 and C2 are described in the text. The dotted line gives the input foreground angular spectrum.

frequency $\nu_{\rm t}$ and extrapolated to a frequency $\nu_{\rm o}$ from which the information on CMB is basically extracted. Thus for synchrotron, if one can use data internal to the BPol experiment, $\nu_{\rm t}$ should be identified with the lowest frequency channel; otherwise it should be the frequency of some other experiment such as Planck. Clearly, the calculations that we are going to expound should be regarded as a guide to appreciate the factors basically involved in a multifrequency experiment.

For Galactic foregrounds the use of a simple equation like

$$l(l+1)C_l^{fore}/2\pi = [\mathcal{B}_{synch}(\nu/\nu_1)^{2\beta_{synch}} + \mathcal{B}_{dust}(\nu/\nu_2)^{2\beta_{dust}}] \cdot l^m \tag{7}$$

including both synchrotron and dust [78] is probably a rather poor fit to data, but can do the job especially if we consider only the intermediate angular scales. Inspection of Fig. 17 of [78] shows the foreground angular spectra at 22.8 GHz look very regular for both E and B in the range l = 10-200. A normalization of 25 μK^2 at $l = 20$ for the B mode seems rather safe. Although this allows to normalize the synchrotron polarization, an extrapolation down to $\sim 10^2$ GHz simply adopting the best WMAP spectral slope $\beta_{synch} = -2.8$, which is somewhat less steep than the E-mode best-fit slope, may be too pessimistic; therefore we consider also a more favourable situation with $\beta_{synch} = -3.1$. For dust one can use either a power-law frequency spectrum or some other model such as in Finkbeiner et al. [79]. Here their model 8 is assumed. Figure 12 compares the angular spectra of synchrotron and dust at 100 GHz, as well the noise BPol spectrum with $\theta_{\rm FWHM} = 30'$.

According to ref. [91], the residual polarization angular spectra of one foreground, evaluated at $\nu_{\rm o}$, are the sums of two terms denoted by $C_{Xl}^{\mathcal{R}_1}$ and $C_{Xl}^{\mathcal{R}_2}$ (where $X = E$, B), which respectively arise from the fluctuation spectrum C_l^β of the spectral index β and the (white) noise spectrum C_l^{noise} in the foreground template:

$$C_{Xl}^{\mathcal{R}_1} = [\ln(\nu_{\rm t}/\nu_{\rm o})]^2 \sum_{l,l'} \alpha_{ll'} C_{Xl}^{fore} C_{l'}^\beta, \qquad C_{Xl}^{\mathcal{R}_2} = C_l^{noise} (\frac{\nu_{\rm o}}{\nu_{\rm t}})^{2\beta}. \tag{8}$$

(Simple corrections can be made in Eq. 8 when β is not independent of frequency.) The spectral index dispersion σ_β and the noise per pixel $\sigma_{\rm t}$ in the template are then given by

$$\sigma_\beta^2 = \frac{1}{4\pi} \sum (2l+1) W_l C_l^\beta, \qquad \sigma_{\rm t}^2 = C_l^{noise}/\Omega_{pixel}. \tag{9}$$

The interpretation of σ_β depends on the way the spectral index field is used. If we extrapolate the template from $\nu_{\rm t}$ to $\nu_{\rm o}$ with the sky-averaged spectral index, then σ_β is the true spectral index fluctuation in the sky (case C1 in the notation of [91]). The slope of the resulting angular spectrum $C_{Xl}^{\mathcal{R}_1}$ is essentially the one of the underlying foreground. A reasonable estimate is $\sigma_\beta = 0.2$. However, if we measure β at each pixel, then σ_β depends on the data noise, and the C_l^β in Eq. 9 denote white noise rather than true structures (case C2). Figure 13 compares the behaviours of $C_{Xl}^{\mathcal{R}_1}$ for both cases. Since the dotted line is the input spectrum we can quickly appreciate the goodness of the suppression, except for a factor $[\ln(\nu_{\rm t}/\nu_{\rm o})]^2$ which remains as small as 1.2 for $\nu_{\rm t}/\nu_{\rm o} = 3$. Case C2 (which is normalized to $\sigma_\beta = 0.1$) looks much better for $l < 10^2$. However the choice in not arbitrary: If we are looking for a resolution of 0.5°, BPol internal data cannot be used to background removal in the intermediate-l region; thus Case C1 applies. If the foreground removal is attempted with a 2° resolution, then one can refer to Case C2. In both cases the $C_{Xl}^{\mathcal{R}_2}$ term is to be added.

The method of [91] allows to compute the residual Galactic backgrounds but does not do the same for extragalactic radio sources and gravitational lensing, for which assumptions must be made. If radio sources can be removed with $S > 300$ mJy the residual source noise at 100 GHz is expected to be $C_l^{RS} = 1.57 \cdot 10^{-7}$ μK^2. If gravitational lensing can be reduced by a factor 10 (cfr. [80]) then its gravitational spectrum at 100 GHz should be less than that of

Case	$\theta^{\rm radio}_{\rm FWHM}$	f_{sky}	σ_{100} (μK)	σ_{30} (μK)	σ_{143} (μK)	r_{lim}
1	0.5°	0.74	0.1	2.1	0.1	$8.0 \cdot 10^{-4}$
2	2°	0.74	0.025	0.167	0.025	$1.0 \cdot 10^{-3}$
3	0.5°	0.12	0.1	2.1	0.1	$1.9 \cdot 10^{-3}$
4	0.5°	0.06	0.1	2.1	0.1	$2.7 \cdot 10^{-3}$

Table 4: Experimental configurations and resulting limits on r at 3σ. Case 2 uses only internal data; in the other cases the 30 GHz noise is adapted to Planck. The 100 GHz angular spectrum of synchrotron is assumed to be $C_l^{synch} = 0.10 l^{-2.6}$ μK^2.

Case	$\theta^{\rm radio}_{\rm FWHM}$	ν_{low} (GHz)	σ_{100} (μK)	$\sigma_{\nu_{low}}$ (μK)	σ_{143} (μK)	r_{lim}
1b	0.5°	30	0.1	2.1	0.1	$9.8 \cdot 10^{-4}$
2b	2°	30	0.025	0.167	0.025	$1.2 \cdot 10^{-3}$
1c	0.5°	40	0.1	2.1	0.1	$1.6 \cdot 10^{-3}$
2c	2°	40	0.025	0.167	0.025	$1.2 \cdot 10^{-3}$

Table 5: Experimental configurations and resulting limits on r at 3σ. Cases 2b and 2c use only internal data; in the other cases the 30 and 40 GHz noise is adapted to Planck. The 100 GHz angular spectrum of synchrotron is assumed to be $C_l^{synch} = 0.24 l^{-2.6}$ μK^2.

radio sources (and roughly with a similar shape), except when radio sources are removed down to the 150 mJy limit: In this case the two contributions are comparable; see the rigth panel in Fig. 12.

Tables 4 and 5 summarize the experimental configurations used in the following computations. Whenever the radio-region angular resolution is $\theta^{\rm radio}_{\rm FWHM} = 2°$ (as for Case 2 in Table 4), only internal data from BPol are assumed to be available, so the noise levels for three channels at 30, 100 and 143 GHz are adjusted to the BPol draft guidelines. When $\theta^{\rm radio}_{\rm FWHM} = 0.5°$, then the lowest frequency noise is adjusted to Planck. Cases 1 and 2, as well as all cases in Table 5, allow the comparison of results for full-sky surveys (with 74% of the sky effectively used). Cases 3 and 4 consider the investigation of small patches of the sky (12% and 6% respectively) with the local angular spectra of both sinchrotron and dust reduced respectively by a factor 5 and 50. The pixel noise is kept equal to the noise of full sky surveys.

Within each Table, the foreground scenario is kept fixed, whereas different data sets are used. In Table 5 the lowest frequency channel for Cases 1c and 2c is raised up to $\nu = 40$ GHz. Comparing the first two lines in Table 5 to those in Table 4, we should consider the only input change is the increased synchrotron foreground.

Figures 14 and 15 report the residual error bars in the CMB angular spectra for the cases with $\nu_{low} = 30$ GHz; the errors are evaluated in the bands [2,10], [11,30], [31,50], [51,90], [140,200], and [201,360]. Clearly even for r as low as $\sim 10^{-2}$ (one order of magnitude below what might be limited by Planck) the intermediate scale spectrum can be detected with a great accuracy and a good harmonic resolution at least near the main spectral bump (which, we recall, is quite stable with respect to τ), or more precisely for $10 \lesssim l \lesssim 100$.

Comparing Case 1 with Case 2, we find moderate differences: using a better resolution (by a factor 4) at the expense of the higher noise for radio receivers makes things somewhat better in the intermediate-l region, but much worse at low l. Inspection of Cases 3 and 4 shows that using the foreground spectra in relatively small patches with a low emission does not seem to help if the noise per pixel is the same. However, the required observation time is much less. Finally, comparing Cases 1a and 2b respectively with 1 and 2 shows that a conservative assumption on Galactic synchrotron has not a dramatic effect after all. The inspection of the last row in Tables 4 and 5 clearly shows that only moderate changes occur in the efficiency in

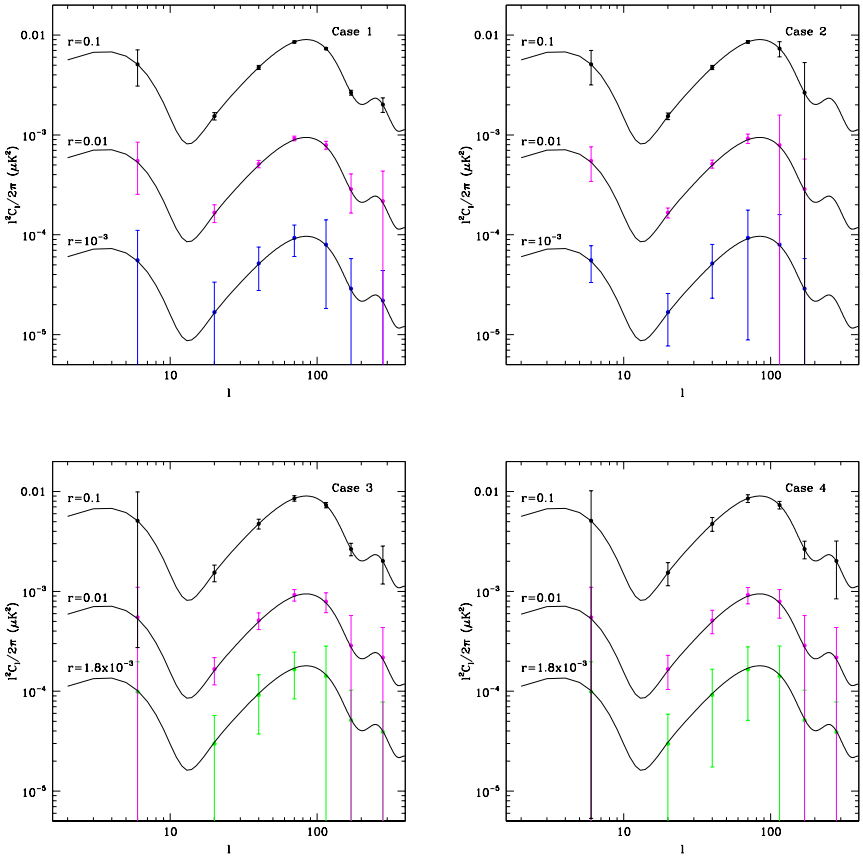

Figure 14: The CMB angular spectrum of B-mode with residual errors after foreground subtraction. The 1-σ errors are computed for the bands described in the text. Cases 1 to 4 refer to the experimental configurations of Table 4.

the measurement of r_{lim}.

Due to the limitations of the present approach we cannot attach an excessive meaning to small differences appearing in Tables 4 and 5. Differences of a factor ~ 2 are still meaningful, but is not so for those of order $\sim 20\%$ arising when we compare the use of internal data to Planck's input at 0.5°. In this case it may be more important, in our view, to get sufficient information from the experiment rather than relying on external data. However, a very interesting fact is that Planck and BPol appear to be complementary in the accurate investigation of different angular scales. A very satisfactory spectral analysis (including the first two spectral bumps) seems to be possible even for r as low as 10^3 when data from both experiments can be put together; in this case low-frequency data should be used from both experiments, combining the advantages of a better noise and a better resolution to some extent. However, due to the limitations of the present data analysis approach, the possible outcome of this solution in terms of $r_{\rm lim}$ is not considered in the above Tables. From the present calculations, we can safely conclude that using external data only (e.g. Planck) makes us lose information on the individual harmonic strengths at $l < 10$ for $r \simeq 1 \cdot 10^{-3}$. (The low-frequency data points in the Figures refer to the full [2,10] band.) In this case, only the use of high-sensitivity internal data at low frequency can recover this part of the spectrum, and this important by itself independently of the fits for r.

Another question is the comparison of BPol configurations with the lowest frequency channel placed at 30 or 40 GHz. Entries 2b and 2c in Table 5 show no appreciable difference for $r_{\rm lim}$. This applies to the more unfavourale normalization for the synchrotron foreground. One might wonder how much this is due to assumption that σ_β is the same in both cases. Should

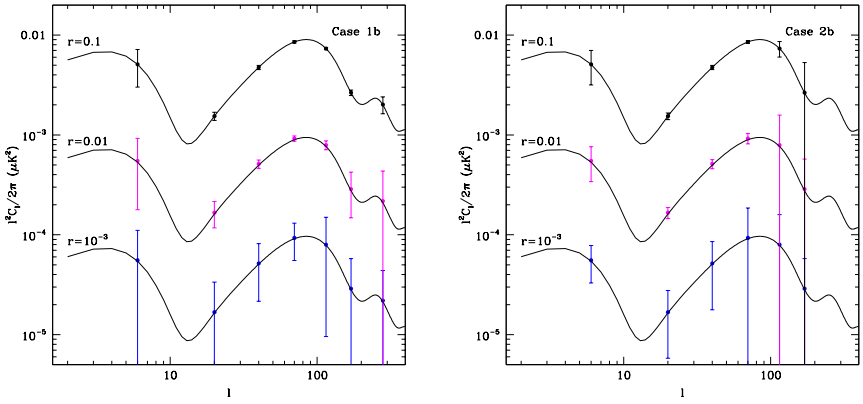

Figure 15: The CMB angular spectrum of B-mode with residual errors after foreground subtraction. Cases 1b and 2b refer to the experimental configurations of Table 5.

synchrotron be the dominant foreground elsewhere, a simple calculation shows that for a couple of frequencies $\nu_{high} > \nu_{low}$

$$\sigma_\beta \approx \frac{\sigma_{high}}{S_{high}}[\ln(\frac{\nu_{high}}{\nu_{low}})]^{-1}, \tag{10}$$

with σ/S the noise-to-signal ratio. In this case using a common ν_{high} we migh have some improvement in σ_β with the 30 GHz channel (by a factor $\lesssim 1.5$). But since synchrotron does not dominate around 100 GHz, the improvement is expected to be much less. Therefore, other considerations can determine the choice since, as remarked in October at Orsay [81], a small change in the r limit produces a much smaller change in our knowledge of the energy scale of inflation.

References

[1] D.N. Spergel et al., "Wilkinson Microwave Anisotropy Probe (WMAP) Three Year Results: Implications for Cosmology", astro-ph/0603449 (2006).

[2] D.N. Spergel et al., "First Year WMAP Observations: Determination of Cosmological Parameters", Ap.J. Supp. 148, 161 (2003).

Bernardi G., Carretti E., Sault R.J., Cortiglioni S., Poppi S., 2006, MNRAS, 370, 2064

Brouw W., Spoelstra T.A.T., 1976, A&AS, 26, 129

Carretti E., McConnell D., McClure-Griffiths N.M., Bernardi G., Cortiglioni S., Poppi S., 2005, MNRAS Letters, 360, L10

Carretti E., Poppi S., Reich W., Reich P., Fürst E., Bernardi G., Cortiglioni, S., Sbarra, C., 2006, MNRAS, 367, 132

Carretti E., Bernardi G., Cortiglioni S., 2006b, MNRAS Letters, 373, L93

La Porta L., Burigana C., 2006, A&A, 457, 1

La Porta L., Burigana C., Reich W., Reich P., 2006, A&A, 455, L9

La Porta L., 2007, PhD Thesis, Bonn University

Reich W., 2007, in "Cosmic magnetismn" ed. R. Fabbri, Research Signpost, in press (astro-ph 0603465)

Testori J.C., Reich P., Reich W., 2007, A$A, in prep.

Wolleben M., Landecker, T.L., Reich W., Wielebinski R., 2006, A&A, 448, 411

[3] Aller, M. F., Aller, H. D., Hughes, P. A., Latimer, G. E. 1999. Centimeter-Wavelength Total Flux and Linear Polarization Properties of Radio-loud BL Lacertae Objects. Astrophysical Journal 512, 601-622.

[4] Argüeso, F., Sanz, J.L., Barreiro, R.B., Herranz, D., González-Nuevo, J., "Statistical analysis of undetected point sources in cosmic microwave background maps", 2006, MNRAS, Volume 373, Issue 1, pp. 311-320 (astro-ph/060934).

[5] Blain, A. W., Chapman, S. C., Smail, I., Ivison, R. 2005. Clustering of Submillimetre-Selected Galaxies. Multiwavelength Mapping of Galaxy Formation and Evolution 94.

[6] Burke, S., Ekers, R. D., Massardi, M., Partridge, B., Ricci, R., Sadler, E. M., In preparation.

[7] Condon, J. J., Cotton, W. D., Greisen, E. W., Yin, Q. F., Perley, R. A., Taylor, G. B., Broderick, J. J. 1998. The NRAO VLA Sky Survey. Astronomical Journal 115, 1693-1716.

[8] de Zotti, G., Gruppioni, C., Ciliegi, P., Burigana, C., Danese, L. 1999. Polarization fluctuations due to extragalactic sources. New Astronomy 4, 481-488.

[9] De Zotti, G., Ricci, R., Mesa, D., Silva, L., Mazzotta, P., Toffolatti, L., González-Nuevo, J., "Predictions for high frequency radio surveys of extragalactic sources", 2005, A&A, 431, 893

[10] González-Nuevo, J., Argüeso, F., Lopez-Caniego, M., Toffolatti, L., Sanz, J.L., Vielva, P., Herranz, D., "The Mexican Hat Wavelet Family. Application to point source detection in CMB maps", 2006, Monthly Notices of the Royal Astronomical Society, 369, 1603.

[11] Granato, G.L., De Zotti, G., Silva, L., Bressan, A., Danese, L., "A physical model for the co-evolution of QSOs and of their spheroidal hosts", 2004, ApJ, 600, 580

[12] Greaves, J. S., Holland, W. S. 2002. Submillimetre polarization of M82 and the Galactic Center: Implications for CMB polarimetry. AIP Conf. Proc. 609: Astrophysical Polarized Backgrounds 609, 267-270.

[13] Greaves, J. S., Holland, W. S., Jenness, T., Hawarden, T. G. 2000. Magnetic field surrounding the starburst nucleus of the galaxy M82 from polarized dust emission. Nature 404, 732-733.

[14] Gregorini, L., Vigotti, M., Mack, K.-H., Zoennchen, J., Klein, U. 1998. Multi-frequency study of the B3-VLA sample I. 10.6-GHz data. Astronomy and Astrophysics Supplement Series 133, 129-147.

[15] Hinshaw, G. et al., "Three-Year Wilkinson Microwave Anisotropy Probe (WMAP) Observations: Temperature Analysis", 2007, ApJ submitted (astro-ph/0603451).

[16] Jones, T. W., Rudnick, L., Fiedler, R. L., Aller, H. D., Aller, M. F., Hodge, P. E. 1985. Magnetic field structures in active compact radio sources. Astrophysical Journal 290, 627-636.

[17] Klaas, U., Laureijs, R. J., Clavel, J. 1999. Far-Infrared Polarization of the Quasar 3C 279. Astrophysical Journal 512, 157-161.

[18] Klein, U., Mack, K.-H., Gregorini, L., Vigotti, M. 2003. Multi-frequency study of the B3-VLA sample. III. Polarisation properties. Astronomy and Astrophysics 406, 579-592.

[19] Komatsu, E. et al., "First-Year Wilkinson Microwave Anisotropy Probe (WMAP) Observations: Tests of Gaussianity", 2003, The Astrophysical Journal Supplement Series, Volume 148, Issue 1, pp. 119-134

[20] Kühr, H., Witzel, A., Pauliny-Toth, I. I. K., Nauber, U. 1981. A catalogue of extragalactic radio sources having flux densities greater than 1 Jy at 5 GHz. Astronomy and Astrophysics Supplement Series 45, 367-430.

[21] Lopez-Caniego, M., Herranz, D., González-Nuevo, J., Sanz, J.L., Barreiro, R.B., Vielva, P., Argüeso, F., Toffolatti, L., "Comparison of filters for the detection of point sources in *Planck* simulations", 2006, MNRAS, 370, 2047.

[22] Lopez-Caniego, M., González-Nuevo, J., Herranz, D., Massardi, M., Sanz, J.L., De Zotti, G., Toffolatti, L., Argüeso, F., "Non-blind catalogue of extragalactic point sources from the Wilkinson Microwave Anisotropy Probe (WMAP) first 3year survey data", 2006, The Astrophysical Journal Supplement Series, in press (astro-ph/0701473).

[23] Mesa, D., Baccigalupi, C., De Zotti, G., Gregorini, L., Mack, K.-H., Vigotti, M., Klein, U. 2002. Polarization properties of extragalactic radio sources and their contribution to microwave polarization fluctuations. Astronomy and Astrophysics 396, 463-471.

[24] Negrello, M., Magliocchetti, M., Moscardini, L., De Zotti, G., Granato, G. L., Silva, L. 2004. Confusion noise at far-infrared to millimetre wavelengths. Monthly Notices of the Royal Astronomical Society 352, 493-500.

[25] Negrello, M., Perrotta, F., González-Nuevo, J., Silva, L., De Zotti, G., Granato, G. L., Baccigalupi, C., Danese, L. 2007. Astrophysical and Cosmological Information from Large-scale sub-mm Surveys of Extragalactic Sources. Monthly Notices of the Royal Astronomical Society submitted.

[26] Okudaira, A., Tabara, H., Kato, T., Inoue, M. 1993. Radio polarization observations of a complete sample of core-dominated radio sources. Publications of the Astronomical Society of Japan 45, 153-166.

[27] Ricci, R., Prandoni, I., Gruppioni, C., Sault, R. J., De Zotti, G. 2004. High-frequency polarization properties of southern Kühr sources. Astronomy and Astrophysics 415, 549-558.

[28] Ricci, R., Sadler, E. M., Ekers, R. D., Staveley-Smith, L., Wilson, W. E., Kesteven, M. J., Subrahmanyan, R., Walker, M. A., Jackson, C. A., De Zotti, G. 2004. First results from the Australia Telescope Compact Array 18-GHz pilot survey. Monthly Notices of the Royal Astronomical Society 354, 305-320.

[29] Sadler, E. M., and 14 colleagues 2006. The properties of extragalactic radio sources selected at 20GHz. Monthly Notices of the Royal Astronomical Society 371, 898-914.

[30] Scott, S. E., Dunlop, J. S., Serjeant, S. 2006. A combined re-analysis of existing blank-field SCUBA surveys: comparative 850-μm source lists, combined number counts, and evidence for strong clustering of the bright submillimetre galaxy population on arcminute scales. Monthly Notices of the Royal Astronomical Society 370, 1057-1105.

[31] Seiffert, M., Borys, C., Scott, D., Halpern, M., "An upper limit to polarized submillimetre emission in Arp 220", 2007, MNRAS, 374, 409

[32] Siebenmorgen, R., Krügel, E., Laureijs, R. J. 2001. The infrared continuum radiation of NGC 1808. A PAH and polarisation study. Astronomy and Astrophysics 377, 735-744.

[33] Tegmark, M., de Oliveira-Costa, A., "Removing Point Sources from Cosmic Microwave Background Maps", 1998, Astrophysical Journal Letters v.500, p.L83

[34] Tucci, M., Martínez-González, E., Toffolatti, L., González-Nuevo, J., De Zotti, G. 2004. Predictions on the high-frequency polarization properties of extragalactic radio sources and implications for polarization measurements of the cosmic microwave background. Monthly Notices of the Royal Astronomical Society 349, 1267-1277.

[35] Tucci, M., Martínez-González, E., Vielva, P., Delabrouille, J. 2005. Limits on the detectability of the CMB B-mode polarization imposed by foregrounds. Monthly Notices of the Royal Astronomical Society 360, 935-949.

[36] Vigotti, M., Gregorini, L., Klein, U., Mack, K.-H. 1999. Multi-frequency study of the B3-VLA sample. II. The database. Astronomy and Astrophysics Supplement Series 139, 359-376.

[37] Argüeso, F., Sanz, J.L., Barreiro, R.B., Herranz, D., González-Nuevo, J., "Statistical analysis of undetected point sources in cosmic microwave background maps", 2006, MNRAS, Volume 373, Issue 1, pp. 311-320 (astro-ph/060934).

[38] González-Nuevo, J., Argüeso, F., Lopez-Caniego, M., Toffolatti, L., Sanz, J.L., Vielva, P., Herranz, D., "The Mexican Hat Wavelet Family. Application to point source detection in CMB maps", 2006, Monthly Notices of the Royal Astronomical Society, 369, 1603 (astro-ph/0604376).

[39] Hinshaw, G. et al., "Three-Year Wilkinson Microwave Anisotropy Probe (WMAP) Observations: Temperature Analysis", 2007, ApJ submitted (astro-ph/0603451).

[40] Komatsu, E. et al., "First-Year Wilkinson Microwave Anisotropy Probe (WMAP) Observations: Tests of Gaussianity", 2003, The Astrophysical Journal Supplement Series, Volume 148, Issue 1, pp. 119-134

[41] Lopez-Caniego, M., González-Nuevo, J., Herranz, D., Massardi, M., Sanz, J.L., De Zotti, G., Toffolatti, L., Argüeso, F., "Non-blind catalogue of extragalactic point sources from the Wilkinson Microwave Anisotropy Probe (WMAP) first 3year survey data", 2006, The Astrophysical Journal Supplement Series, in press (astro-ph/0701473).

[42] Tegmark, M., de Oliveira-Costa, A., "Removing Point Sources from Cosmic Microwave Background Maps", 1998, Astrophysical Journal Letters v.500, p.L83

[43] Bennett, C.L. *et al.*, ApJS, 148, 97, 2003.

[44] Planck Consortia, The, "Planck: the Scientific Programme", ESA-SCI(2005)-1, (2005).

[45] `http://southpoletelescope.uchicago.edu/`

[46] Ruhl, J.E. *et al*, 2004, arXiv:astro-ph//0411122.

[47] Ruhl, J.E., 2007, private communication.

[48] R. Ricci et al., 'High-frequency polarization properties of southern Kühr sources', A&A, 415, 549 (2004)

[49] M.L. Lister, D.C. Homan, 'MOJAVE: Monitoring of Jets in Active Galactic Nuclei with VLBA Experiments. I. First-Epoch 15 GHz Linear Polarization Images', AJ, 130, 1389 (2005)

[50] A.R. Taylor et al., 'Radio polarimetry of the ELAIS N1 field: polarized compact sources', submitted to AJ (2007)

[51] M. Tucci et al., 'Predictions on the high-frequency polarization properties of extragalactic radio sources and implications for polarization measurements of the cosmic microwave background', MNRAS, 349, 1267 (2004)

[52] D. Messa et al., 'Polarization properties of extragalactic radio sources and their contribution to microwave polarization fluctuations', A&A, 396, 463 (2002)

[53] R. Cen, 'Grand unification II: Hot accretion and AGN jets', astro-ph/0702660 (2007)

[54] P. Coles, P. Dineen, J. Earl & D. Wright, "Phase Correlations in Cosmic Microwave Background Sky Maps", Mon. Not. R. astr. Soc., 350, 989 (2004)

[55] L.-Y. Chiang, P. Coles, P.D. Naselsky & P. Olesen, "The One-dimensional Fourier Representation and Large Angular Scale Foreground Contamination in the 3-year Wilkinson Microwave Anisotropy Probe Data", JCAP, 01, 021 (2007)

[56] L.-Y. Chiang, P.D. Naselsky & P. Coles, "Testing the Gaussian Random Hypothesis with the Cosmic Microwave Background Temperature Anisotropies in the Three-Year WMAP data", ApJ Letters, in press, astro-ph/0603662 (2007)

[57] . Dineen & P. Coles, "A Faraday Rotation Template for the Galactic Sky", Mon. Not. R. astr. Soc., 362, 403 (2005)

[58] D.N. Spergel et al., "Wilkinson Microwave Anisotropy Probe (WMAP) Three Year Results: Implications for Cosmology", astro-ph/0603449 (2006).

[59] D.N. Spergel et al., "First Year WMAP Observations: Determination of Cosmological Parameters", Ap.J. Supp. 148, 161 (2003).

[Benoit et al. (2002)] Benoit, A., P., Ade, A., Amblard et al. 2002 *Astropart. Phys.* 17, 101–124

[Benoit et al. (2004a)] Benoit, A. et al. 2004, Å424, 571-582

[60] Finkbeiner D., Davis M., Schlegel D.J. 1999, ApJ 524, 867

[61] Bernard et al. 2007 in "Sky polarization at Far-Infrared to Radio wavelengths: the cosmoc screen before the CMB", M.A. Miville Deschê nes and F. Boulanger Eds, 23, 189.

[62] Vaillancourt 2007 in "Sky polarization at Far-Infrared to Radio wavelengths: the cosmoc screen before the CMB", M.A. Miville Deschê nes and F. Boulanger Eds, 23, 147.

[63] Meny C., Gromov V., Boudet N., Bernard J.P. et al. 2007, accepted in A&A (astro-ph/0701226)

[Fosalba et al. (2002)] Fosalba P., Lazarian A., Prunet S., Tauber J.A., 2002, ApJ, 564, 762

[Heiles (2000)] Heiles C., 2000, AJ, 119, 923

[Zweibel & Heiles (1997)] Zweibel E.G., Heiles C., 1997, New Astronomy, 235, 131

[Page et al. (2006)] Page, L., Hinshaw, G., Komatsu, E., et al. 2006, ApJ, in press, astro-ph/0603450

[Hinshaw et al. (2006)] Hinshaw, G., Nolta, M. R., Bennett, C. L., et al. 2006, ApJ, in press, astro-ph/0603451

[64] Brouw W.N., Spoelstra T.A.T., 1976, A&AS, 29,129

[65] Duncan A.R., Haynes R.F., Jones K.L., Stewart R.T., 1997, MNRAS, 291, 279

[66] Wolleben M., Landecker T.L., Reich W., Wielebinski R., 2006, A&A, 448, 411

[67] Bernardi G., Carretti E., Cortiglioni S., Sault R.J., Kesteven M.J., Poppi S., 2003, ApJ, 594, 5

[68] Carretti E., McConnell D., McClure-Griffiths N.M., Bernardi G., Cortiglioni S., Poppi S., 2005, MNRAS, 360, 10

[69] Bernardi G. Carretti E., Sault R.J., Cortiglioni S., Poppi S., 2006, MNRAS, 370, 2064

[70] Carretti E., Poppi S., Reich W., Reich P., Furst E., Bernardi G., Cortiglioni S., Sbarra C., 2006, MNRAS, 367, 132

[71] Tucci M., Carretti E., Cecchini S., Fabbri R., Orsini M., Pierpaoli E., 2000, NewA., 5, 181

[72] Bernardi G. Carretti E., Fabbri R., Sbarra C., Poppi S., Cortiglioni S., Jonas J.L., 2004, MNRAS, 351, 436

[73] Carretti E.,Bernardi G., Sault R.J., Cortiglioni S., Poppi S., 2005, MNRAS, 358, 1

[74] La Porta L., Burigana C., Reich W., Reich P., 2006, A&A, 455, L9

[75] Benoit A., et al., 2004, A&A, 424, 571

[76] http://lambda.gsfc.nasa.gov/product/map/current/parameters.cfm

[77] M. Tucci et al., "Limits on the detectability of the CMB B-mode polarization imposed by foregrounds", MNRAS 360, 935 (2005)

[78] L. Page et al., "Three year Wilkinson Anisotropy Probe (WMAP) observations: polarization analysis", http://lambda.gsfc.nasa.gov, (2006)

[79] D.P. Finkbeiner, M. Davis and D.J.Schlegel, "Extrapolation of Galactic dust emission at 100 μm to cosmic microwave background radiation frequencies using FIRAS", ApJ 524, 867 (1999)

[80] L. Knox and Y.S. Song, "Limit on the detectability of the energy scale of inflation", Phys. Rev. Lett. 89, 011303 (2002)

[81] K. Land et al., Bpol Meeting, Orsay, October 2006

[82] F. Argüeso, J. González-Nuevo & L. Toffolatti L. "Contributions of Point Extragalactic Sources to the Cosmic Microwave Background Bispectrum", 203, ApJ, 598, 86

[83] F. Argüeso, J.L. Sanz, R.B. Barreiro, D. Herranz & J. González-Nuevo, "Statistical analysis of undetected point sources in cosmic microwave background maps", 2006, MNRAS, 373, 311

[84] D. Babich & M. Zaldarriaga, "Primordial bispectrum information from CMB polarization", 2004, Phys. Rev. D, 70, 083005

[85] L.-Y. Chiang, P.D. Naselsky, O.V. Verkhodanov & M.J. Way, "Non-Gaussianity of the Derived Maps from the First-Year Wilkinson Microwave Anisotropy Probe Data", 2003, ApJ, 590, L65

[86] C.J. Copi, D. Huterer & G.D. Starkman, "Multipole vectors: A new representation of the CMB sky and evidence for statistical anisotropy or non-Gaussianity at 2¡=l¡=8", 2004, Phys. Rev. D, 70, 043515

[87] M. Cruz, E. Martínez-González, P. Vielva & L. Cayón, "Detection of a non-Gaussian spot in WMAP", 2005, MNRAS, 356, 29

[88] A. de Oliveira-Costa, M. Tegmark, M. Zaldarriaga & A. Hamilton, "Significance of the largest scale CMB fluctuations in WMAP", 2004, Phys. Rev. D 69, 063516

[89] H.K. Eriksen, F.K. Hansen, A.J. Banday, K.M. Górski & P.B. Lilje, "Asymmetries in the Cosmic Microwave Background Anisotropy Field", 2004, ApJ, 605, 14

[90] E. Komatsu et al., "First-Year Wilkinson Microwave Anisotropy Probe (WMAP) Observations: Tests of Gaussianity", 2003, ApJS, 148, 1, 119

[91] M. Tucci, E. Martínez-González, P. Vielva & J. Delabrouille, "Limits on the detectability of the CMB B-mode polarization imposed by foregrounds", 2005, MNRAS, 360, 935

[92] P. Vielva, E. Martínez-González, R.B. Barreiro, J.L. Sanz & L. Cayón, "Detection of Non-Gaussianity in the Wilkinson Microwave Anisotropy Probe First-Year Data Using Spherical Wavelets", 2004, ApJ, 609, 22

[93] Y. Wiaux, P. Vielva, E. Martínez-González & P. Vandergheynst, "Global Universe Anisotropy Probed by the Alignment of Structures in the Cosmic Microwave Background", 2006, Phys. Rev. Lett., 96, 151303

[94] M. Lopez-Caniego, J. González-Nuevo, D. Herranz, M. Massardi, J.L., Sanz, G. De Zotti, L. Toffolatti, F. Argüeso, "Non-blind catalogue of extragalactic point sources from the Wilkinson Microwave Anisotropy Probe (WMAP) first 3year survey data", ApJS, in press (astro-ph/0701473).

[Amari and Chichocki(1998)] Amari S., Chichocki A., 1998, Proc. IEEE, 86, 2026

[Baccigalupi et al.(2000)] Baccigalupi, C.; Bedini, L.; Burigana, C.; De Zotti, G.; Farusi, A.; Maino, D.; Maris, M.; Perrotta, F.; Salerno, E.; Toffolatti, L.; Tonazzini, A., Monthly Notices of the Royal Astronomical Society, Volume 318, Issue 3, pp. 769-780, 2000

[Baccigalupi et al.(2004)] Baccigalupi, C.; Perrotta, F.; de Zotti, G.; Smoot, G. F.; Burigana, C.; Maino, D.; Bedini, L.; Salerno, E., Monthly Notices of the Royal Astronomical Society, Volume 354, Issue 1, pp. 55-70, 2004

[Donzelli et al.(2006)] Donzelli, S.; Maino, D.; Bersanelli, M.; Childers, J.; Figueiredo, N.; Lubin, P. M.; Meinhold, P. R.; O'Dwyer, I. J.; Seiffert, M. D.; Villela, T.; Wandelt, B. D.; Wuensche, C. A., Monthly Notices of the Royal Astronomical Society, Volume 369, Issue 1, pp. 441-448, 2006

[Finkbeiner et al.(1999)] Finkbeiner, Douglas P.; Davis, Marc; Schlegel, David J., The Astrophysical Journal, Volume 524, Issue 2, pp. 867-886, 1999

[Haslam et al.(1982)] Haslam, C. G. T.; Salter, C. J.; Stoffel, H.; Wilson, W. E., Astronomy and Astrophysics Supplement Series, vol. 47, Jan. 1982, p. 1, 2, 4-51, 53-142, 1982

[Hinshaw et al.(2007)] Hinshaw, G.; Nolta, M. R.; Bennett, C. L.; Bean, R.; Dor, O.; Greason, M. R.; Halpern, M.; Hill, R. S.; Jarosik, N.; Kogut, A.; Komatsu, E.; Limon, M.; Odegard, N.; Meyer, S. S.; Page, L.; Peiris, H. V.; Spergel, D. N.; Tucker, G. S.; Verde, L.; Weiland, J. L.; Wollack, E.; Wright, E. L., The Astrophysical Journal in press, 2007, astro-ph/0603451

[Hyvarinen and Oja(1999)] Hyvarinen A., Oja E., 1999, Independent Component Analysis: A Tutorial http://www.cis.hut.fi/∼aapo/papers/IJCNN99_tutorialweb/

[Maino et al.(2002)] Maino, D.; Farusi, A.; Baccigalupi, C.; Perrotta, F.; Banday, A. J.; Bedini, L.; Burigana, C.; De Zotti, G.; Grski, K. M.; Salerno, E., Monthly Notices of the Royal Astronomical Society, Volume 334, Issue 1, pp. 53-68, 2002

[Maino et al.(2003)] Maino, D.; Banday, A. J.; Baccigalupi, C.; Perrotta, F.; Grski, K. M., Monthly Notice of the Royal Astronomical Society, Volume 344, Issue 2, pp. 544-552, 2003

[Maino et al.(2007)] Maino, D.; Donzelli, S.; Banday, A. J.; Stivoli, F.; Baccigalupi, C., Monthly Notices of the Royal Astronomical Society, Volume 374, Issue 4, pp. 1207-1215, 2007

[Stivoli et al.(2006)] Stivoli, F.; Baccigalupi, C.; Maino, D.; Stompor, R., Monthly Notices of the Royal Astronomical Society, Volume 372, Issue 2, pp. 615-629, 2006

[95] Carretti E., Bernardi G., Cortiglioni S., 2006, MNRAS Letters, 373, L93

[96] Page L., et al., 2006, ApJ, submitted, astro-ph/0603450

[97] Ponthieu N., et al., 2005, A&A, 444, 327

[98] Reich W., 2006, astro-ph/0603465

[99] Testori J.C., Reich P., Reich W., 2004, in *The Magnetized Interstellar Medium*, ed. by B. Uyanıker, W. Reich, R. Wielebinski, (Copernicus GmbH, Katleburg-Lindau 2004) p. 57

[100] Wolleben M., Landecker T.L., Reich W., Wielebinski R., 2006, A&A, 448, 411

Ponthieu et al. Astron.Astrophys. 444 (2005) 327 (astro-ph/0501427)

Bedini et al. (2005)EURASIP Journal on Applied Signal Processing, 15, 2400

Bonaldi et al. Mon.Not.Roy.Astron.Soc. 373 (2006) 263-270 (astro-ph/0609701)